4

Final Report

UNDEREXPANDED NONCONDENSING TURBULENT GAS JETS IN LIQUIDS

by

E. Loth and G.M. Faeth
Department of Aerospace Engineering
The University of Michigan
Ann Arbor, Michigan 48109-2140

Prepared for:

Department of the Navy
Officer of Naval Research
Propulsion and Energetics (Code 1132P)
800 N. Quincy Street
Arlington, Virginia 22217-5000

Contract No. N00014-85-0604
G.D. Roy
Scientific Program Officer

August 1988

Unclassified

SECURITY CLASSIFICATION OF THIS PAGE (When Data Entered)

REPORT DOCUMENTATION PAGE		READ INSTRUCTIONS BEFORE COMPLETING FORM
1. REPORT NUMBER	2. GOVT ACCESSION NO.	3. RECIPIENT'S CATALOG NUMBER
4. TITLE (and Subtitle) Underexpanded Noncondensing Gas Jets in Liquids		5. TYPE OF REPORT & PERIOD COVERED Final Report 8/1/85 - 8/30/88
		6. PERFORMING ORG. REPORT NUMBER
7. AUTHOR(s) E. Loth and G.M. Faeth		8. CONTRACT OR GRANT NUMBER(s) N00014-85-K-0604
9. PERFORMING ORGANIZATION NAME AND ADDRESS Department of Aerospace Engineering The University of Michigan Ann Arbor, MI 48109-2140		10. PROGRAM ELEMENT, PROJECT, TASK AREA & WORK UNIT NUMBERS Work Unit NR 097-464
11. CONTROLLING OFFICE NAME AND ADDRESS Office of Naval Research 800 North Quincy Street Arlington, VA 22217-5000		12. REPORT DATE August 1988 13. NUMBER OF PAGES 70 + ix pp.
14. MONITORING AGENCY NAME & ADDRESS(if different from Controlling Office)		15. SECURITY CLASS. (of this report) Unclassified 15a. DECLASSIFICATION/DOWNGRADING SCHEDULE
16. DISTRIBUTION STATEMENT (of this Report) Approved for public release; distribution unlimited.		
17. DISTRIBUTION STATEMENT (of the abstract entered in Block 20, if different from Report)		
18. SUPPLEMENTARY NOTES		
19. KEY WORDS (Continue on reverse side if necessary and identify by block number) Multiphase flow, gas jets, in liquids, compressible turbulent jets. (orig.)		

20. ABSTRACT (Continue on reverse side if necessary and identify by block number)

The structure of turbulent noncondensing round and plane air jets submerged in still water were investigated experimentally. Both adapted and underexpanded jets were considered, the latter with underexpansion ratios up to 8:1. Measurements included flow visualization, using flash photography and shadowgraphs as well as high-speed motion-picture photography; mean void fraction distributions, using gamma-ray absorption; entrainment rates, using laser-Doppler anemometry; and mean static pressures, using static-pressure

DD FORM 1 JAN 73 1473 EDITION OF 1 NOV 65 IS OBSOLETE
S/N 0102-LF-014-6601

Unclassified

SECURITY CLASSIFICATION OF THIS PAGE (When Data Entered)

probes. Present measurements and the earlier results of Bell et al. (1972), Tross (1974) and Carreau et al. (1985) were used to evaluate analysis of the process. The analysis was based on the locally-homogeneous-flow approximation (relative velocities between the phases neglected) and the effective-adapted-jet approximation for underexpanded jets.

Shadowgraphs of plane underexpanded jets and static pressure measurements for both round and plane underexpanded jets showed the presence of a shock-wave-containing external-expansion region for underexpanded air jets in water, similar to underexpanded air jets in air. Effects of acoustic feedback observed for underexpanded air jets in air disappeared for underexpanded air jets in water due to the different acoustic properties of the multiphase mixing layer near the jet exit. The visual widths of air jets in water are unusually large because of the strong sensitivity of void fractions to mixing levels due to the large density ratio of the flow. Predictions agreed reasonably well with measurements, except for adapted jets where intrinsic unsteadiness enhanced mixing rates; and very near the jet exit for underexpanded jets, where deflections of the mixing layer due to the presence of shock cells cannot be treated using the effective-adapted-jet approximation.

TABLE OF CONTENTS

ACKNOWLEDGEMENTS

The authors wish to acknowledge the assistance of the staff of the Gas Dynamics Laboratories of the Department of Aerospace Engineering for assistance with the experiments; especially Roger Glass, Clete Iott, Warren Eaton and Thomas Griffin. The assistance of T.-Y. Sun, now of Parker-Hannifin Corporation of Cleveland, Ohio, during the initial phases of the investigation, and S.G. Chuech, now of CFD Inc. of Huntsville, Alabama for assistance with the analysis, is also appreciated. We also thank Clete Iott for valuable technical assistance with flow visualization techniques, and Deborah Adams for help in preparing this report.

LIST OF TABLES

LIST OF FIGURES

NOMENCLATURE

a	acceleration of gravity
b	plane injector exit width
C_i	constants in turbulence model
C_e	dimensionless entrainment coefficient
d	jet exit diameter
d_e	equivalent jet exit diameter
f	mixture fraction
F_e	streamwise thrust on passage
g	square of mixture fraction fluctuations
k	turbulence kinetic energy
$\dot{m}_o$	passage flow rate
$\dot{m}$	jet mass flow rate
M	Mach number
M_c	convective Mach number
p	pressure
$P(f)$	probability density function of mixture fraction
r	radial distance
r_e	characteristic flow width
Re	passage exit Reynolds number
Ri	passage exit Richardson number
Sc	laminar Schmidt number
S_ϕ	source term in governing equations
T	temperature
u	streamwise velocity
v	radial velocity
x	streamwise distance
y	lateral distance from plane of symmetry of jet
Y_i	mass fraction of species i
α	void fraction
β_∞	angle between the jet boundary and the axis
γ	specific heat ratio
δ_{IC}	width of initial mixed layer
ε	rate of dissipation of turbulence kinetic energy
μ	laminar viscosity

μ_{eff}	effective viscosity
μ_t	turbulent viscosity
ρ	density
σ_i	turbulent Prandtl/Schmidt number
ϕ	generic property

Subscripts

a	air
c	centerline value
e	effective exit condition
s	sonic-adapted flow
w	water
o	passage exit condition
∞	ambient condition
0.5	value at $\bar{\alpha} = 0.5$

Superscripts

j	= 1 for axisymmetric flow, = 0 for plane flow
t	stagnation condition
(-), (-)'	time-averaged mean and root-mean-squared fluctuating quantity
(~)(~)''	Favre-averaged mean and root-mean-squared fluctuating quantity

1. Introduction

This investigation considered the structure and mixing properties of round and plane vertical noncondensing gas jets in liquids, motivated by application involving metal processing, direct-contact condensers, gas dissolution systems, reservoir distratification systems, liquid-metal combustors, and nuclear reactor pressure-suppression systems – among others. The main objective was to provide new measurements of flow structure and mixing properties, however, the new measurements were also used to evaluate past proposals for analyzing the process. The first phase of the study considered initial measurements and analysis of round jets (Loth & Faeth, 1987); the present investigation involved additional measurements and analysis of both round jets and plane jets. Supplementary work under this investigation considering the structure of gas jets in gases, has also been reported by Chuech (1987) and Chuech et al. (1987, 1988).

Gas jets submerged in liquids are complicated by effects of unsteadiness at low flow rates, similar to the pulsitile behavior of highly buoyant single-phase flows. This involves oscillatory release of gas which can cause liquid to slug into the jet passage. The unsteadiness is accompanied by appreciable fluctuations of static pressures in the flow passage and beyond the jet boundaries, often resulting in excessive noise and vibration as well as blockage of passage in cases where the gas reacts with the liquid (Kerney et al., 1972; Chan, 1974; Avery & Faeth, 1974).

Effects of unsteadiness can be reduced by increasing gas flow rates in the passage, frequently leading to operation with underexpanded jets, where the flow is sonic and the static pressure is greater than the ambient pressure at the jet exit. It is well known that static pressure equalization for underexpanded gas jets in gases occurs in an external-expansion region near the jet exit – involving shock waves and other compressible-flow phenomena (Shapiro, 1954). Moiseev (1962) and Surin et al. (1983) observed that dynamic pressures along the axis of underexpanded gas jets in gases and liquids were similar while static pressures along the axis of underexpanded gas jets in gases and liquids were also found to be similar during the first phase of this investigation (Loth and Faeth, 1987). These observations suggest that a multiphase external-expansion region, involving gas dynamic phenomena, is present for underexpanded gas jets in liquids as well.

In view of the complexities of unsteadiness at low flow rates, and the presence of the external-expansion region at high flow rates, current understanding of gas injection into liquids is not very complete; nevertheless, the flow has received some

attention in the past. Earlier work in this laboratory considered round jets, including the following: noncondensing gas jets in liquids (Tross, 1974); condensing gas jets in liquids (Kerney et al., 1972; Weimer et al., 1973; Chen & Faeth, 1982); and reacting gas jets in liquids (Avery & Faeth, 1974; Chen & Faeth, 1983). The earliest experimental studies were confined to gross parameters like the length of the vapor-or-gas-containing region of condensing or reacting jets (Kerney et al., 1972; Weimer et al., 1973; Avery & Faeth, 1974). Analysis was also undertaken based on an integral model of turbulence and the locally-homogeneous flow (LHF) approximation of multiphase flow theory (Soo, 1967). The LHF approximation implies infinitely-fast interphase transport rates and local thermodynamic equilibrium between the phases, i.e., velocity differences between the phases are neglected and phase and chemical equilibrium are assumed to be maintained at each point within the flow. Gas-dynamic processes in multiphase flows are not well understood; therefore, the complexities of the external-expansion region were avoided by defining effective-adapted-jet exit conditions, where the static pressure at the passage exit was the same as the ambient pressure. This approach was reasonably successful for correlating the length of the vapor-or gas-containing region of condensing jets (Kerney et al., 1972; Weimer et al., 1973; Avery & Faeth, 1974).

Tross (1974) measured mean void fractions, using an electrical conductivity probe, and dynamic pressures, using an impact probe, in adapted and underexpanded air jets in still water. The flow was analyzed similar to Weimer et al. (1973) and Avery & Faeth (1974). Unfortunately, the analysis was not very effective for predicting flow structure in spite of its earlier success. This was attributed to the uncertainty of probe measurements in multiphase flows as well as problems of treating a rapidly developing flow, having a large density ratio, with an integral model (Tross, 1974).

Subsequent work in this laboratory considered a higher-order turbulence model in an effort to improve predictions (Chen & Faeth, 1982, 1983). The conserved-scalar formalism of Bilger (1976) and Lockwood & Naguib (1975) was used, which had provided a successful treatment of constant density, variable density, and combusting turbulent jets during other work in this laboratory (Jeng & Faeth, 1984). The LHF approximation was adopted, while only flow rates slightly in excess of the sonic condition were considered to avoid problems of external expansion. A key feature of the combined use of the LHF and the conserved-scalar approximations is that scalar properties (void fraction, density, etc.) are only functions of mixture fraction (the fraction of mass at a point which originated from the injector). These functions, called state relationships, can be found from straight forward adiabatic mixing or adiabatic

reaction calculations, typical of fundamental thermodynamic theory. Use of the turbulence model and LHF approximations was successful for predicting the length of the vapor- or gas-containing region of both condensing and reacting jets, with all empirical parameters of the turbulence model fixed at values appropriate for constant-density single-phase jets (Chen & Faeth, 1982, 1983). The same approach has been evaluated for a variety of other multiphase jets, see Faeth (1987) and references sited therein. In general, the approach was reasonably successful in dense multiphase flows but tended to overestimate the rate of development of dilute dispersed flows where finite interphase transport rates become important and the LHF approximation fails.

Based on these findings the same approach was examined during the first phase of the present investigation (Loth & Faeth, 1987). These measurements involved adapted and underexpanded round air jets injected vertically upward in still water, with underexpansion ratios (the ratio of jet exit to ambient static pressures or the ratio of initial jet mass flow rates to the initial jet mass flow rate for sonic-adapted conditions at the jet exit) up to 8. It was judged to be premature to consider the complexities of a shock-wave-containing multiphase external expansion region; therefore, effective-adapted-jet exit conditions were used, following Kerney et al. (1972). This was justified by recent measurements of Birch et al. (1984, 1987), Chuech (1987) and Chuech et al. (1987, 1988) which showed that effective-adapted-jet exit conditions provide an effective treatment of the structure of underexpanded gas jets in gases, even quite close to the external expansion region itself. Because of the rapid development of the flow for gas injection into liquids, resulting from the large density ratio (Chen & Faeth, 1982, 1983) the extent of the external expansion region should be smaller for gas/liquid than gas/gas systems, favoring the approximation as well. The comparison between predicted and measured time-averaged void fraction distributions was moderately successful – particularly at high underexpansion ratios. For adapted and subsonic exit conditions, however, large-scale and pulsitile jet flow was observed which enhanced mixing rates well above predictions. Furthermore, unsteadiness near the jet exit appeared to influence distributions of void fractions even for the highest underexpansion ratios considered. These results highlighted the need to study flow properties near the jet exit in greater detail.

Related studies by others paralleled activities in this laboratory. To begin with round jets, early work by Cumo et al. (1978), Kudo et al. (1974), Lee et al. (1979) and Young et al. (1974) involved measurements of only the gross features of condensing jets, like the length of the vapor-containing region. Relevant portions of this data were used to evaluate LHF analysis of condensing jets (Chen & Faeth, 1982). Bakaklevskii

& Chekhovich (1978) report temperature and dynamic pressure profiles in condensing plane jets in coflow, however, measurement accuracy and flow conditions are too uncertain to provide more than a rough guide to structure. Chan (1974), Chun & Sonin (1984), Lambier & Chow (1984) and Simpson & Chan (1982) measured static pressures near the passage exit for subsonic condensing jets, finding the large pressure pulsations indicative of unsteady flow that were mentioned earlier. Structure measurements are more numerous for noncondensing jets but most results are limited to dilute bubbly flows far from the passage exit (Abdel-Aal et al., 1966; Mahalingen et al., 1976; Ohba et al., 1977 and Ohba, 1979). Past studies of processes near the passage exit generally involve the use of probes or other intrusive techniques, for example: the dynamic pressure measurements of Moiseev (1962) and Surin et al. (1983); measurements of void diameter using a passage plate by Bell et al. (1972); and measurements of entrainment using the water overflow technique by Bell et al. (1972) and Carreau et al. (1983).

The main objective of the present investigation was to extend the measurements of Loth & Faeth (1987) for round jets to consider the near-jet-exit region of plane jets. Adapted and underexpanded vertical plane jets in still water were considered with underexpansion ratios up to 4. The plane jet configuration offered a better opportunity to observe the flow and direct photographs and shadowgraphs were obtained for underexpanded conditions. Other measurements were the same as Loth & Faeth (1987): time-averaged void fractions, using gamma-ray absorption; mean and fluctuating jet exit velocities and entrainment rates, using laser-Doppler anemometry; and static pressures along the plane of symmetry using a static-pressure probe. In addition hydrophone measurements were made in the surrounding liquid near the jet exit to study acoustic phenomena associated with unsteadiness near the passage exit. The present structure measurements, supplemented by earlier measurements of Bell et al. (1972), Carreau et al. (1985) and Tross (1974), were used to evaluate predictions based on past proposals for analyzing this flow, e.g., use of the LHF and effective-adapted-jet approximations (Chen & Faeth, 1982, 1983; Faeth, 1987; Loth & Faeth, 1987).

The report begins with a description of experimental and theoretical methods. Results are then considered, treating flow definition, structure, entrainment and the comparison between predictions and measurements for both round and plane jets. The following discussion is brief, more details and a complete tabulation of data can be found in Loth (1988). Additional publications relating to this research include: Chuech (1987), Chuech et al. (1987, 1988) and Loth & Faeth (1987, 1988).

1. Experimental Methods

2.1 Apparatus

Measurements were carried out in a water-filled tank (1m x 2m x 2m high) which had glass side walls. Figure 1 is a sketch of the arrangement for tests with a round jet. The jets were directed vertically upward and could be traversed in three directions with horizontal and vertical positioning accuracies of 0.1mm and 1mm. The round injectors were located near the center of the tank and were generally at least 650mm below the liquid surface with a liquid depth of 1500mm. In this case flow disturbances at the liquid surface were controlled by wave dampers which yielded wave heights less than 75mm and pressure disturbances near the jet exit less than 2kPa. The plane injector was located near the surface with a liquid depth of 1100mm and wave dampers were not needed.

A sketch of a typical round injector appears in Fig. 2.The injector consisted of a plenum, a honeycomb flow straightener (1.6 mm cells, 25 mm long) and a calming section, all having a diameter of 32 mm, followed by a constant-radius converging section to a constant-diameter flow passage. Two jet passages were used having inside diameters of 4.9 and 11.0 mm and lengths of 230 mm to yield nearly fully-developed pipe flow at the exit. The passages extended into the water as tubes for most of their length and were tapered from the outside to a sharp edge at the exit. Static pressures were measured in the plenum and one diameter upstream of the exit.

A sketch of the plane injector appears in Fig. 3. This consisted of a 140 cm^3 plenum chamber feeding into a honeycomb flow straightener (1.6 mm cells, 20 mm long) followed by three 30 mesh brass screens. The flow then passed through a 6:1 lateral contraction designed to provide a uniform exit velocity (within 1 percent based on potential flow theory). The dimensions of the jet exit were 4.8 mm wide $\times$ 57 mm long, yielding an initial aspect ratio of eleven. Subsequently, plate glass sidewalls provided optical access for a streamwise distance of 13 exit widths and a lateral distance of 16 exit widths. Screens (30 mesh) were placed along the sides of the test section to reduce disturbances while the liquid level was maintained near the top edge of the test section.

The air supply was drawn from laboratory facilities which were filtered and dried to a dewpoint less than 240 K. Air flow rates were controlled with pressure regulators and metered with critical-flow nozzles having diameters of 2.43 and 7.62 mm (Flow Engineering Co., 0.1 percent accuracy). Pressures on the upstream side of the critical-flow nozzles were measured with a 250 mm diameter Heisse pressure gage (0-2 MPa range).

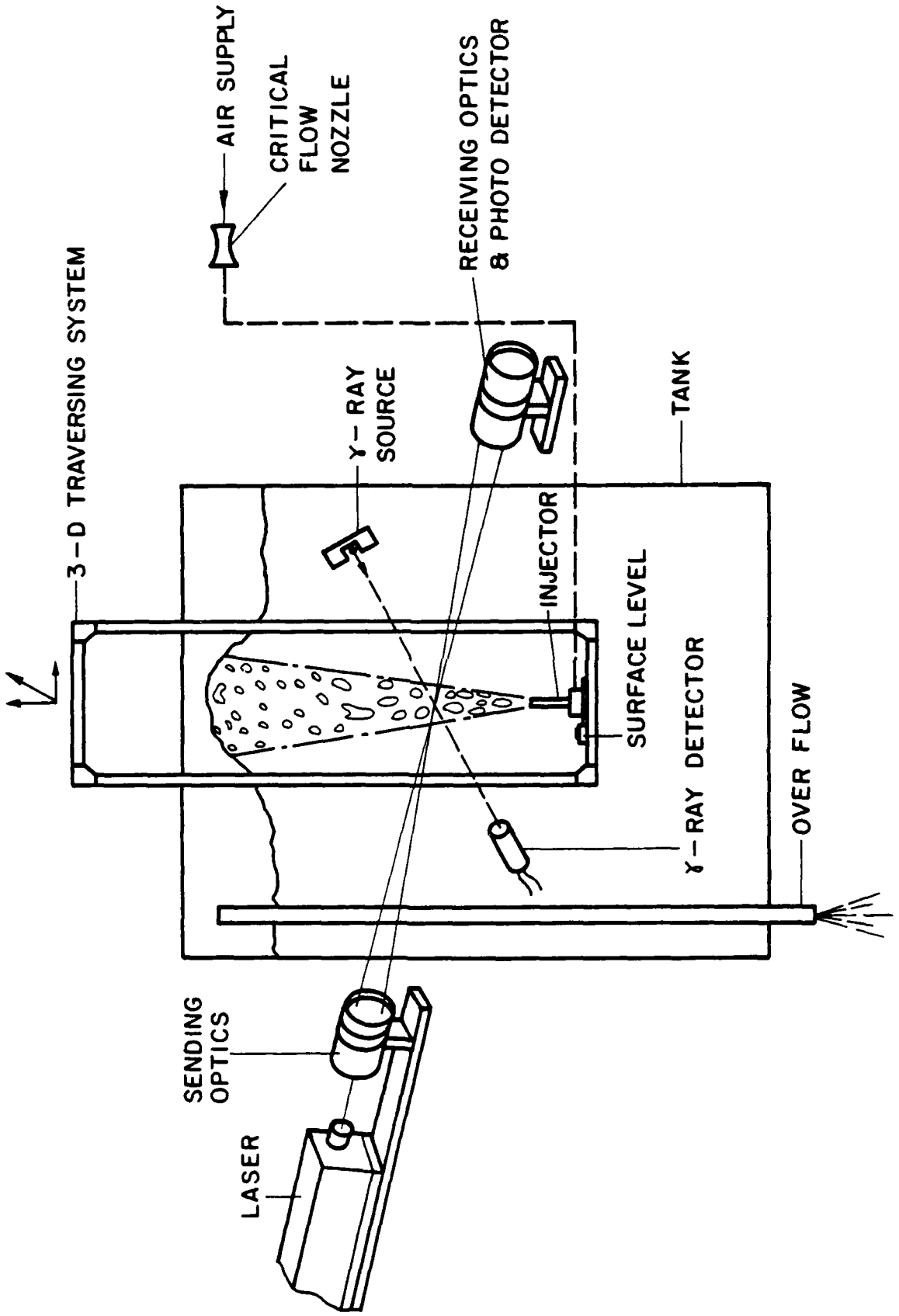

Figure 1. Sketch of test apparatus.

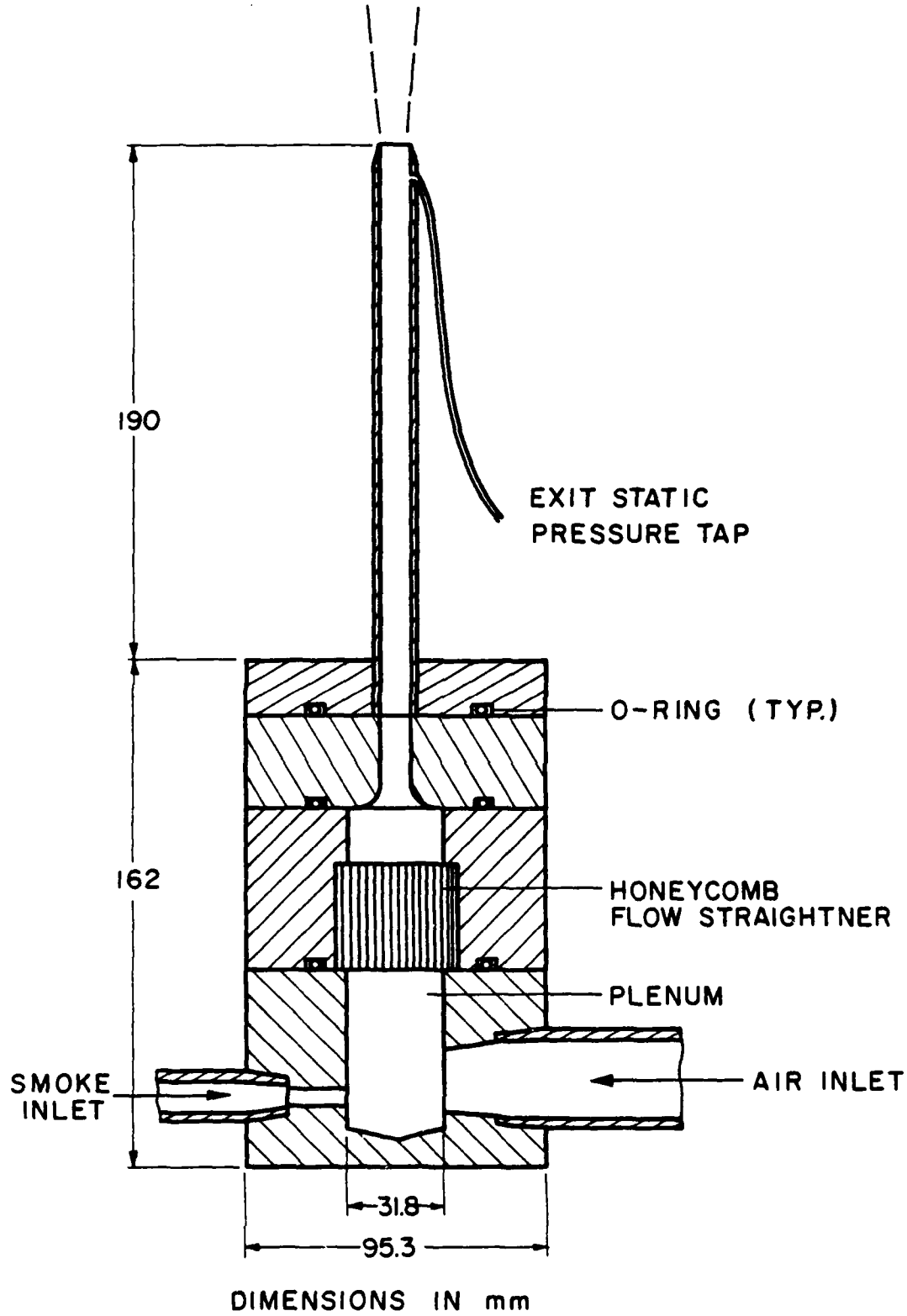

Figure 2. Sketch of round injector.

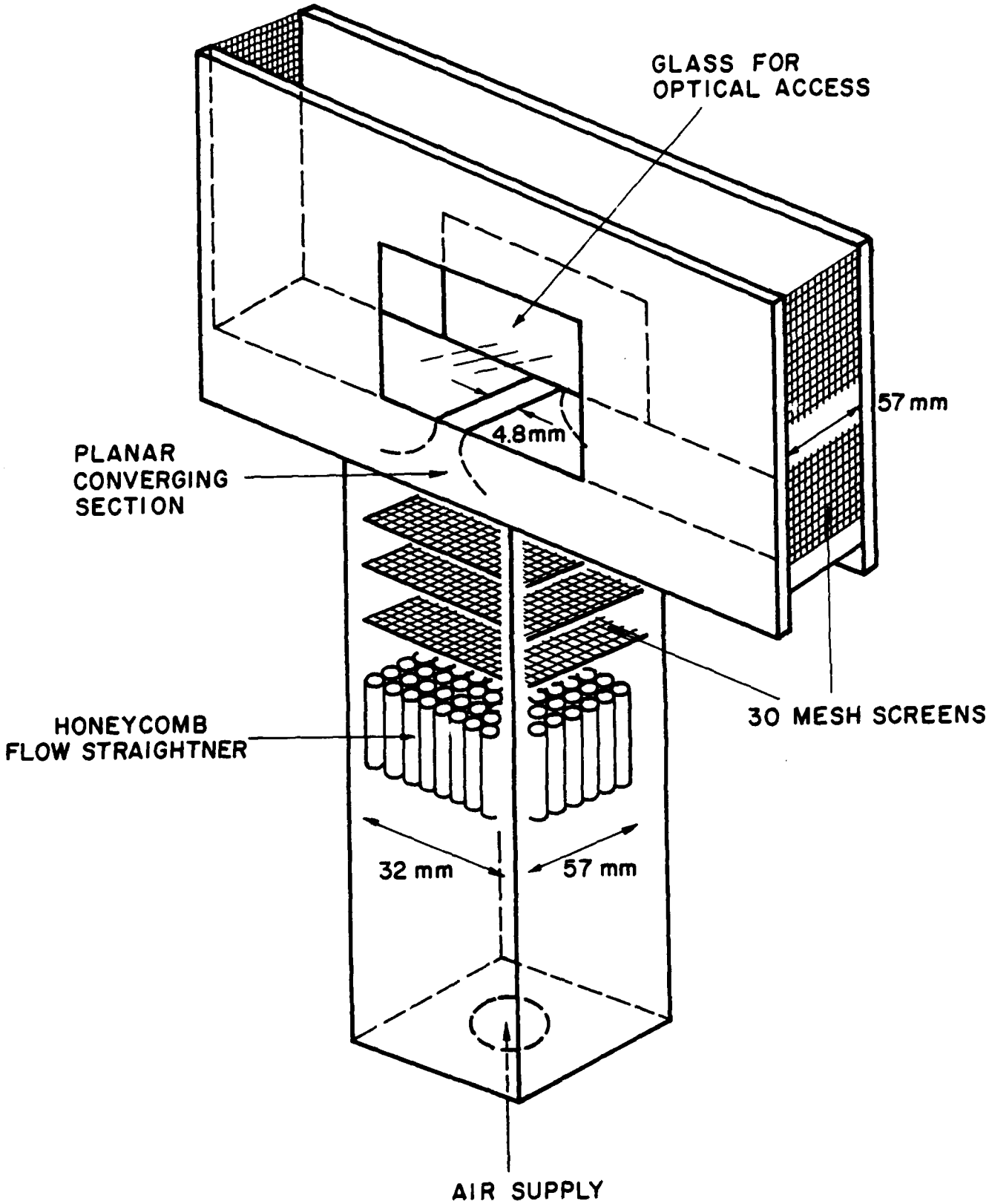

Figure 3. Sketch of plane injector.

2.2 Instrumentation

Flow Visualization. Flash photographs, high-speed motion picture photographs using continuous lighting, and flash shadowgraphs (plane jet only) were used to document the mixing and dynamics of gas release at the jet exit, and to observe the compressible wave field for the plane jets.

Static Pressures. Static pressures were measured along the axis of the 11 mm diameter round jet, and along the center plane of symmetry of the plane jets, using an arrangement similar to Eggers (1966). The arrangement for the round jet is illustrated in Fig. 4.

The static pressure probe consisted of a 1mm diameter stainless-steel tube with the upstream end closed and a 0.4 mm diameter static-pressure tap. The static-pressure tap was located so that it could be traversed over the region $-1 \leq x/d \leq 7$, with a positioning accuracy of 1 mm, where x is the distance from the jet exit and d is the passage exit diameter. The probe was centered along the axis with two supports: one within the passage at $x/d = -6$, the other in the bath at $x/d = 13$. A small air purge was used to keep the probe free of water when measuring air jets in water. The arrangement for the plane jet was similar to the round jet, except that the static pressure tube was supported upstream of the converging section and twenty-five slot widths downstream of the exit while the probe could be traversed in the range $-1 \leq x/b \leq 13$. These probes were only in place when static pressures were measured: no probes were located in the flow field for all other operations. Static pressures were read with a 250 mm diameter Heisse pressure gage (0-2 MPa) and are estimated to have experimental uncertainties (95 percent confidence) less than 30 percent of the pressure difference between the jet and the water bath (Loth, 1988).

It is well known that acoustic feedback can cause instabilities which enhance mixing of underexpanded gas jets in gases (Sherman et al., 1976). This affect was studied using a Spartan Model 110-8459 Hydrophone (2dB response in the range 1-40 kHz) during tests with the 4.9 mm diameter round passage and the plane passage. The hydrophone was positioned in the bath at $x/d = 6$ and r/d or $y/b = 6$. The hydrophone output was processed by averaging 100 power spectral density distributions obtained with a rectangular window and a resolution of 40 Hz.

Void Fractions. Distributions of time-averaged void fractions were measured using gamma-ray absorption. For the round jets, absorption measurements for chord-like paths through the flow, at a given streamwise distance, were deconvoluted to find radial distributions of time-averaged void fraction. Gamma-rays were obtained from a Co-57 source (Amhersham Inc., 2 mCi, 271 day half-life) placed in a lead casket, with

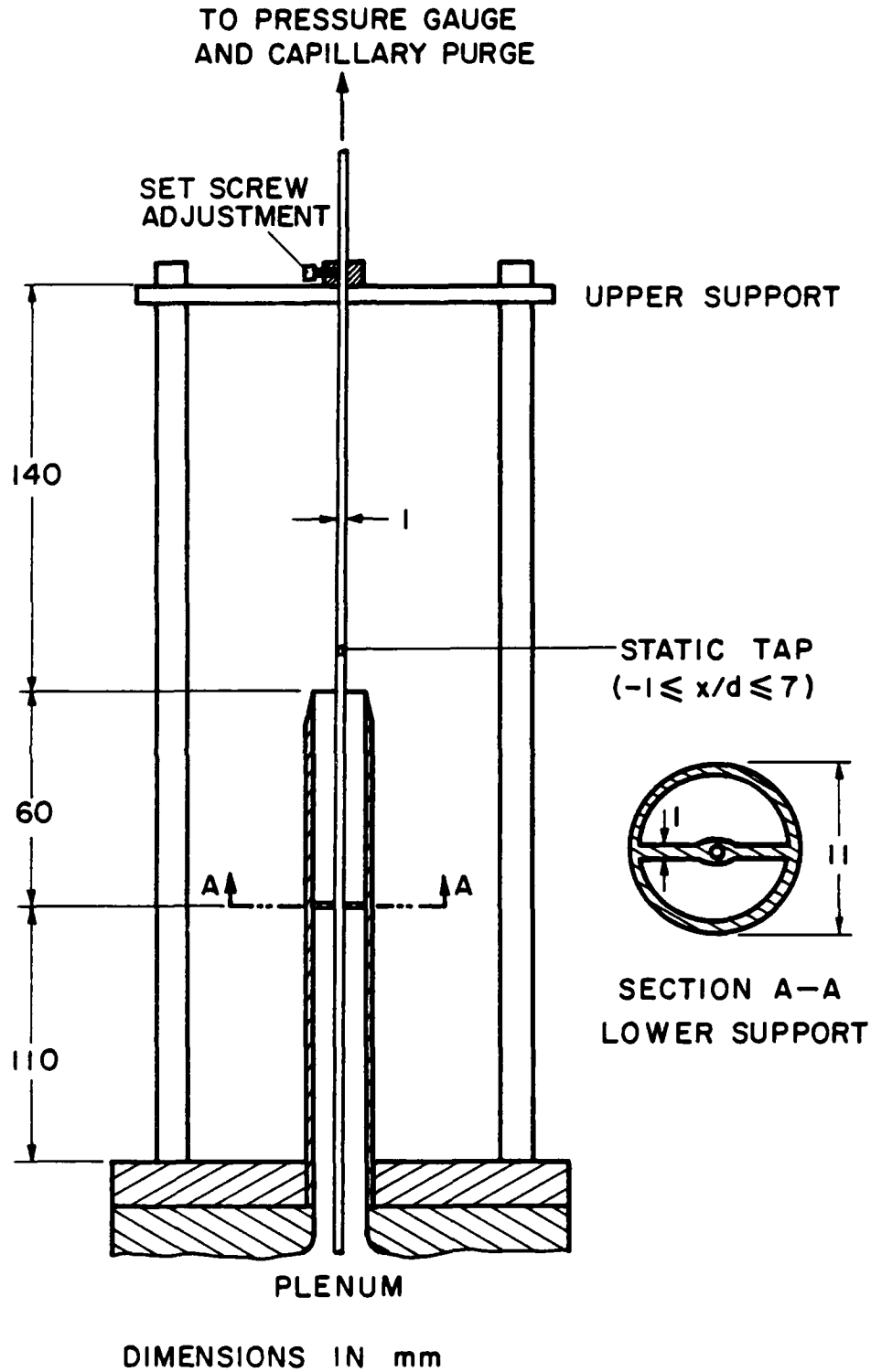

Figure 4. Sketch of static-pressure probe.

an output beam of gamma-rays directed across the flow using a lead collimator (2 mm diameter and 13 mm long). After traversing the flow, the beam passed through a lead aperature (2, 3, and 5 mm diameter, depending on the jet width, and 13 mm long) to the detector (EG & G Model 905-1 sodium iodide scintillator and photomultiplier). The detector signal was preamplified and then processed by an EG & G Model 590A single-channel analyzer and amplifier, and an EG & G Model 974 timer/counter. The output counts of the timer/counter were then collected and stored, for various sampling times, using an IBM-AT computer. The absorption window of the detector was 114-128 keV, to capture the 122 keV emission of the source while eliminating low energy background radiation. The source and detector were located on either side of the jet flow, submerged in the tank in waterproof housings. At each axial position, absorption measurements were obtained for 20-40 horizontal chord-like paths through the flow. Roughly 10,000 counts were accumulated for each path which required sampling times of 8-50 minutes. The linear absorption coefficient of gamma-rays for air is about four orders of magnitude smaller than for water; therefore, the logarithm of the counting rate is proportional to the fraction of air in the radiation path. Assuming axisymmetric flow, the absorption measurements were deconvoluted, following Santoro et al. (1981), to obtain radial profiles of time-averaged void fraction.

The arrangement for the plane jet measurements was very similar to the round jets, except that the source was replaced by a 10 mm Ci source to shorten test times. Naturally, in this case the measurements could be used directly and no deconvolution was necessary.

Bias errors of the void fraction measurements are influenced by whether liquid laminae in the absorption path are parallel or normal to the path (Ohba, 1979). Low intensity ratios reduced uncertainties due to this effect to less than 5 percent, based on the findings of Ohba (1979). Dynamic bias errors, due to turbulent fluctuations of void fractions along the path, were estimated by deconvolutions through a linearized error analysis, which showed bias errors of less than 5 percent.

The main source of experimental uncertainty for the round jets was amplification of count rate uncertainty during deconvolution. This was calculated using the matrix model of Limbaugh & Kneile (1984) for results obtained by deconvolution of data with a prescribed uncertainty. This resulted in experimental uncertainties (95 percent confidence) at the centerline of less than 20 percent, with relative uncertainties increasing inversely proportional to the indicated mean void fraction at off-axis positions. Since no deconvolution was necessary for the plane jets, their experimental uncertainties were lower, less than 10 percent. Assessment of errors, based on

retrieving a mean void fraction of unity for several positions in the jet air core, confirmed uncertainty estimates within these limits (Loth, 1988).

Velocities. A conventional dual beam, frequency-shifted, forward-scatter, laser-Doppler anemometer (LDA) was used to measure mean and fluctuating streamwise velocities at the injector exit (with the tank empty) and mean jet entrainment velocities in the liquid. The uncertainties of the entrainment velocity measurements (95 percent confidence) are estimated to be less than 10 percent (Loth, 1988).

Entrainment. Jet entrainment rates, defined as the rate increase of the mass flow rate of the jet with the streamwise distance, were obtained from the entrainment velocity measurements. These measurements were made along the jet boundaries outside the gas-containing region at a radial distance r_∞ or lateral distance y_∞ while correcting for low levels of streamwise velocity, u_∞, in the region where accurate measurements of radial velocity, v_∞, could be made. Based on these measurements, the rate of increase of the mass flow rate of the jet, $\dot{m}$ with streamwise distance is:

$$d\dot{m}/dx = (2\pi r_\infty)^j \rho_\infty (\bar{u}_\infty \tan \beta_\infty - \bar{v}_\infty); \; j = 1 \text{ (round)} = 0 \text{ (plane)} \qquad (2.1)$$

where ρ denotes density, β_∞ is the angle between the jet boundary and the axis, and an overbar denotes a time average. From this a dimensionless entrainment coefficient can be defined using scaling laws, as follows:

$$C_e \equiv d\dot{m}/dx / (F_e \rho_\infty b^{j-1})^{1/2} \qquad (2.2)$$

where F_e is the streamwise thrust on the passage of the round jet, and is the thrust per unit length for the plane jet.

The term involving $\bar{u}_\infty$ in equation (2.1) contributed less than 10 percent to the entrainment while entrainment rates were relatively independent of the location of y_∞ outside the gas-containing region. Estimated experimental uncertainties (95 percent confidence) of the entrainment measures were less than 20 percent for the round jets and less than 10 percent for the plane jets, largely governed by uncertainties of the velocity measurements and effects of locating r_∞ or y_∞ (Loth, 1988).

2.3 Test Conditions

Test conditions are summarized in Table 1 as a function of underexpansion ratio, $\dot{m}/\dot{m}_s$. For the round jets, flow rates varied from subsonic jets to highly

Table 1 Summary of Test Conditions+

$\dot{m}/\dot{m}_s$	ρ_e(kg/m^3)	$\dot{m}_e$(g/s)	$\dot{F}_e$(N)	Re/10^5 †	Ri/10^{-4} §
4.9 mm injector: (fully-developed pipe flow):					
0.6	1.36	5.28	1.11	0.80	8.14
1.0	1.52	8.68	2.73	1.34	3.31
2.0	3.06	17.5	7.42	3.62	1.21
4.0	6.12	35.8	16.7	8.01	0.54
8.0	12.3	71.7	35.9	17.2	0.25
11.0 mm injector: (fully-developed pipe flow):					
0.6	1.36	26.3	5.53	1.80	18.5
1.0	1.52	43.8	13.8	3.01	7.41
2.0	3.06	87.7	37.3	8.16	2.73
4.0	6.12	174.0	83.6	18.5	1.22
4.8 mm plane injector: (slug flow):					
1.0	1.45	113	35.5	1.22	3.25
2.0	2.90	226	96.3	3.30	0.88
3.0	4.36	339	157	5.40	0.50
4.0	5.82	453	218	7.49	0.34

+Initial conditions for an air jet injected vertically upward in still water having a temperature of 294 ± 2K; ambient pressure at jet exit of 107.5 ± 0.7 kPa. Air stagnation temperature of 295 = 2 K.

†$Re = \rho_e \dot{F}_e d/(\mu_e \dot{m}_e)$.

§$Ri = (\rho_\infty / \rho_e - 1)\, ad(\dot{m}_e / \dot{F}_e)^2$.

underexpanded sonic jets ($0.6 \leq \dot{m}/\dot{m}_s \leq 8.0$). Measurements for the plane jets all involved sonic exit conditions ($1 \leq \dot{m}/\dot{m}_s \leq 4$).

For $\dot{m}/\dot{m}_s \geq 1$, the ratios of the passage exit to ambient static pressures are equal to $\dot{m}/\dot{m}_s$. Flow Reynolds numbers are quite high, ca. 10^5 and the jets were turbulent. Richardson numbers were relatively low, ca. 10^{-4}; therefore, effects of buoyancy were small in the external-expansion region near the passage exit. However, mixing is rapid for air injection into water and the large density difference between water and air causes significant effects of buoyancy farther downstream, $x/d > 20$, for the round jets.

Related measurements from earlier work were also used to examine flow structure. These measurements all involved round jets as summarized in Table 2. The test conditions fall within the range of present measurements for round jets, although measurements were generally made using intrusive methods.

Table 2 Test Conditions for Related Measurements[a]

Source	Bell et al. (1972)	Carreau et al. (1985)	Tross (1974)
Injected Fluid	Nitrogen	Nitrogen	Air
Jet Direction	Horizontal	Horizontal	Vertical
Jet Diameter (mm)	0.5 - 1.7	0.5	3.2 & 6.4
$\dot{m}/\dot{m}_s$	3.5	2-50	1.4 - 14.0
Re x 10^5	0.5 - 2.0	0.3 - 70	0.8 - 5.0
Measurements	Entrainment: Water Overflow Jet Width: Passage Plate	Entrainment: Water Overflow	Void Fraction: Resistivity Probe Dynamic Pressure: Impact Probe.

[a] All round jets using converging nozzles injected into still water at normal temperature and pressure.

3. Theoretical Methods

3.1 General Description

Analysis was similar to the approach proposed by Chen & Faeth (1982, 1983) to treat flows of this type. The method has been evaluated in this laboratory using structure measurements for a wide range of multiphase round jets (see Faeth (1987) and references sited therein): the objective of present work was to extend this evaluation to underexpanded gas jets in liquids.

The three major assumptions of the analysis are as follows: (1) use of the locally-homogeneous flow approximation to treat multiphase flow effects; (2) use of effective-adapted-jet exit conditions to treat the external-expansion region of underexpanded jets; and (3) use of a higher-order turbulence model to treat turbulent mixing. The LHF approximation implies negligible relative velocities between the phases and local thermodynamic equilibrium; therefore, the flow is treated like a single-phase fluid having large density variations due to changes in gas concentrations while separated-flow parameters, like drop and bubble size distributions, do not enter the formulation. Consistent with present limited knowledge concerning the structure of gas jets in liquids, it seems prudent to evaluate the performance of LHF analysis, as a baseline, before undertaking the additional complications of separated-flow analysis. Furthermore, recent evaluations of the LHF approximation suggests reasonably good performance in the near-injector region of round sprays and bubbly jets (Faeth, 1987; Ruff et al., 1988; and Sun & Faeth, 1986): this provides additional motivation for examination of the approach here.

The effective-adapted-jet approximation is frequently used to avoid the complexities of treating gas-dynamic phenomena in external-expansion regions when estimating turbulent mixing for both single- and multi-phase flows (Avery & Faeth, 1974; Birch et al., 1984, 1987; Chuech et al., 1988; Kerney et al., 1972; Weimer et al., 1973). Recent evaluations have also shown that the approach is reasonably effective for estimating the structure of underexpanded gas jets in gases, even close to the external-expansion region (Birch et al., 1984, 1987; Chuech, 1987, Cheuch et al., 1987, 1988). Since present measurements, and those of Surin et al. (1983), suggest that external-expansion regions of underexpanded gas jets in liquids are smaller than for underexpanded gas jets in gases, the region where the approximation is useful should be even larger for the present flows.

Due to the high Reynolds numbers of present flows, some degree of modeling must be accepted to treat their mixing properties. Consistent with past work on gas jets

in liquids and related multiphase jets in this laboratory (Chen & Faeth, 1982, 1983; Faeth, 1987; Ruff et al., 1988; Sun & Faeth, 1986), turbulent mixing was treated using a simplified k-ε-g turbulence model. The approach is similar to an early recommendation by Lockwood & Naguib (1975) but is extended to use mass-weighted (Favre) averages to simplify treatment of density fluctuations as recommended by Bilger (1976). Empirical constants for round jets were based on calibrations for constant- and variable-density single-phase round jets using the Favre-averaged formulation (Jeng & Faeth, 1984), however, the values are not very different from Lockwood & Naguib (1975). Empirical parameters were the same for plane jets, except for use of a modified turbulent Prandtl/Schmidt number as recommended by Lai et al. (1986). This approach is plausible since the present flows are geometrically simple high Reynolds number turbulent flows for which turbulence models were developed and have been reasonably successful. Furthermore, recent evaluation of this approach for the near-injector region of large-scale pressure-atomized sprays has been reasonably successful (Ruff et al., 1988) suggesting some capability to treat large density ratios, comparable to the present flows, as well.

Other major assumptions of the analysis are as follows: steady (in the mean) axisymmetric turbulent jet with no swirl; boundary-layer approximations apply; equal exchange coefficients of all species, phases and heat; buoyancy considered in the governing equations for mean quantities but ignored in the governing equations for turbulence qualities; and effects of mean kinetic energy, viscous dissipation and compressibility are ignored. The first assumption is a condition of the experiments while use of the boundary-layer approximations is not an issue for nonswirling jets. Assuming equal exchange coefficients of all species, dispersed-phases and heat is widely accepted for high Reynolds number turbulent flows where turbulent transport dominates flow properties (Lockwood & Naguib, 1975; Bilger, 1976; Jeng & Faeth, 1984; Faeth, 1987). Neglecting buoyancy in the governing equations for turbulence quantities minimizes empiricism while past work shows that the effect of this approximation is small with respect to mean properties (Jeng & Faeth, 1984). Finally, underexpanded jets involve supersonic flow downstream of the passage exit so that neglecting effects of mean kinetic energy, viscous dissipation and compressibility is clearly questionable. However, the external expansion region is not large and is only treated approximately using the effective-adapted-jet approach; therefore, the added complications of treating these effects are not justified.

3.2 Formulation

Under the assumptions of the analysis, the conserved-scalar formalism can be used (Bilger, 1976). This involves solving governing equations for conservation of mass, mean momentum, mean mixture fraction, turbulence kinetic energy, the rate of dissipation of turbulence kinetic energy, and mixture fraction fluctuations squared. All quantities are formulated in terms of Favre averages, which are defined as follows:

$$\tilde{\phi} = \overline{\rho\phi} / \bar{\rho} \tag{3.1}$$

where an overbar indicates a conventional time average. By this definition $\phi = \tilde{\phi} + \phi''$, where $\overline{\rho\phi''} = 0$, but $\bar{\phi}'' \neq 0$ necessarily, unless the density is constant.

The Favre-averaged governing equations can be written in the following form:

$$r^j\partial/\partial x\,(\bar{\rho}\tilde{u}\,\phi) + \partial/\partial r\,(r^j\rho v\phi) = \partial/\partial r\,((r^j\mu_t/\sigma_\phi)\,\partial\phi/\partial r) + r^j S_\phi \tag{3.2}$$

where $j = 1$ for round jets and $j = 0$ for plane jets. While lateral variations are denoted $\partial(\,)/\partial r$ for the plane jet by this notation, they should be recognized to imply $\partial(\,)/\partial y$. The dependent variable ϕ is a generic variable where $\phi = 1$ (for conservation of mass), $\tilde{u}$, $\tilde{f}$, k, ε and g (*where k, ε and g are Favre-averaged quantities in this formulation*). The source terms, S_ϕ, and the appropriate empirical constants are summarized in Table 3. As noted earlier, the only difference in the round and plane jet formulation involves changing $\sigma_f = \sigma_g$ from 0.7 (for round jets) to 0.5 (for plane jets) as recommended by Lai et al. (1986). The turbulent viscosity is calculated in the usual manner:

$$\mu_t = C_\mu\bar{\rho}k^2/\varepsilon \tag{3.3}$$

Table 3. Summary of Source Terms in the Governing Equations

ϕ	$\mu_{eff,\phi}$	S_ϕ
1	--	0
$\tilde{\mu}$	$\mu + \mu_t$	$a\,(\rho_\infty - \bar{\rho})$
$\tilde{f}$	$(\mu/Sc) + (\mu_t/\sigma_f)$	0
k	$\mu + (\mu_t/\sigma_k)$	$\mu_t(\partial\,\tilde{u}/\partial r)^2 - \bar{\rho}\,\varepsilon$
ε	$\mu + (\mu_t/\sigma_\varepsilon)$	$[C_{\varepsilon 1}\mu_t\,(\partial\,\tilde{u}/\partial r)^2 - C_{\varepsilon 2}\,\bar{\rho}\,\varepsilon]\,\varepsilon/k$
g	$(\mu/Sc) + (\mu_t/\sigma_g)$	$C_{g1}\mu_t\,(\partial\,\tilde{f}/\partial r)^2 - C_{g2}\,\bar{\rho}\,g\varepsilon/k$

C_μ	$C_{\varepsilon 1}$	C_{g1}	$C_{\varepsilon 2} = C_{g2}$	σ_k	σ_ε	$\sigma_f = \sigma_g$	Sc
0.09	1.44	2.8	1.87	1.0	1.3	0.7 (j=1) 0.5 (j=0)	0.7

3.3 Initial Conditions

Several effective-adapted-jet approximations have been proposed to treat the mixing properties of underexpanded jets while avoiding the complications of the external-expansion region, see Chuech et al. (1988) for a review of methods proposed thus far. The divergent-nozzle approach of Kerney et al. (1972) was used during the present investigation. This involves replacing the actual external-expansion process by isentropic flow to the ambient pressure, and applying the new diameter, velocities, etc., of the flow at the exit plane of the actual passage - ignoring the presence of any virtual origin. This approach has been effective for estimating the mixing properties for injection of gases into gases, and conserves mass, momentum and energy for the flow (Chuech et al., 1988). The character of the flow, either fully-developed pipe flow or a low-turbulence (slug) flow, was preserved in this process as recommended by Chuech et al. (1988), however, use of either slug flow or fully-developed flow had a negligible effect on computed results in the region where measurements were made. Formulas for these computations are reported by Loth & Faeth (1987) and are also widely available in the literature, e.g., see Shapiro (1954). This approach will be denoted the equivalent exit condition (EEC) model in the following.

By definition $\tilde{f} = 1$ and $g = 0$ across the jet exit, yielding standard initial conditions. Present measurements, however, suggested enhanced mixing very close to the jet exit due to effects of intrinsic unsteadiness. To represent this effect, a partially-mixed initial condition was also used to obtain a better fit of void fraction distributions and entrainment rates near the jet exit. The mixed initial condition involved a mixing layer having a sinusoidal variation of time-averaged void fraction at the outer edge of the injected fluid as sketched in Fig. 5. The dimensionless thicknesses, δ_{IC}, were 38 percent and 28 percent for the round and plane jets. The time-averaged void fraction distributions were found from the measurements, assuming similarity of the growth rate of mixing layer thickness and extrapolating to x/d or b of 0.25. The associated velocities, mixture fractions and densities were computed based on conservation of momentum for a constant-pressure mixing layer and assuming Dirac delta functions at $f = 0$ and 1 for the probability density function (PDF) of mixture fraction.

Measurements of jet exit conditions for the round jets showed that fully-developed turbulent pipe flow was nearly achieved (Loth & Faeth, 1987). Thus, mean velocity distributions at the jet exit used the power law distributions due to Nikuradese (Hinze, 1975), while measurements due to Laufer were used to specify k and ε

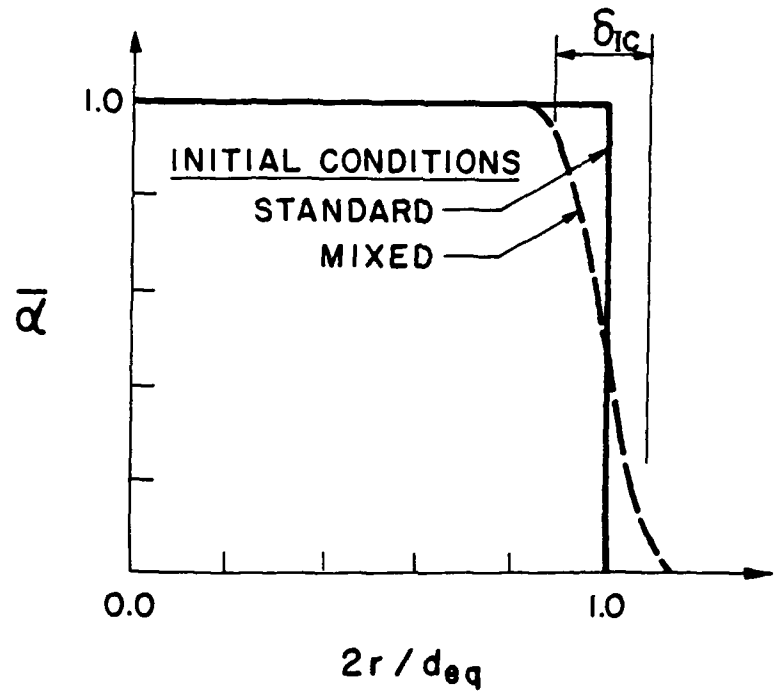

Figure 5. Initial conditions for void fraction for EEC model.

(Schlichting, 1979). The plane jet initial condition approximated slug flow and was taken to be a uniform velocity with a turbulence intensity of less than 3 percent for 99 percent of the flow width.

3.4 State Relationships

When exchange coefficients are equal, and effects of kinetic energy and radiation are small, all instantaneous scalar properties (density, temperature, phase fractions, species concentrations, etc.) are only a function of mixture fraction. This implies that instantaneous scalar properties can be found by straightforward adiabatic mixing (or chemical equilibrium) calculations, where f kg of passage exit fluid and (1-f) kg of ambient fluid are adiabatically mixed and brought to thermodynamic equilibrium. The relationships between scalar properties and f are termed state relationships: several examples of state relationships and their construction appear in the literature (Bilger, 1976; Chen & Faeth, 1982, 1983; Faeth, 1987; Jeng & Faeth, 1984).

In the present case, state relationships constructed for isothermal mixing of air and water neglecting the small vapor pressure of water were found to be adequate; therefore, only this formulation will be shown. The mass fractions of air and water are given as

$$Y_a = f,\ Y_w = 1\text{-}f \tag{3.4}$$

For isothermal mixing, the phase densities remain constant, therefore, the mixture density becomes:

$$\rho = (f/\rho_a + (1\text{-}f) / \rho_w)^{-1} \tag{3.5}$$

Finally, the void fraction is

$$\alpha = \rho f/\rho_a \tag{3.6}$$

In order to evaluate potential effects of additional property variations at high underexpansion ratios, state relationships were also constructed assuming mixing of air at the maximum effective jet exit condition considered during this investigation $\dot{m}/\dot{m}_s$ = 8). Effects of kinetic energy were also ignored for this calculation, with the static state at the passage exit taken to be equal to the ambient pressure. This results in low mixture temperatures so that the formation of ice must be considered.

State relationships for the isothermal mixing and maximum isentropic expansion states are illustrated in Fig. 6. Differences between the two state relationships are only evident at mixture fractions near unity, where ice is formed for isentropic expansion, as noted earlier. During mixing calculations, flow conditions dropped rapidly below mixture fractions where the two state relationships differ; therefore, the simple isothermal mixing approximation was adopted with little error (Loth & Faeth, 1987).

The results illustrated in Fig. 6 show that α is a very nonlinear function of mixture fraction, increasing rapidly with increasing f near f = 0 and then remaining near unity thereafter. This behavior can be quantified by noting that equation (3.6) approaches the following form for small f:

$$\alpha = f\rho_w/\rho_a \text{ , for } f << \rho_a/\rho_w \tag{3.7}$$

Since $\rho_w/\rho_a \sim 10^3$ for present conditions, equation (3.7) implies that α is a very sensitive function of f in this region.

3.5 Scalar Properties

Given state relationships, time-averaged and Favre-averaged scalar properties were computed according to Bilger (1976). This involves finding a Favre-averaged probability density function of mixture fraction, $\tilde{P}(f)$, as described later. Given $\tilde{P}(f)$, the Favre-averaged mean and mean-squared fluctuating values of any scalar property become (Bilger, 1976):

$$\tilde{\phi} = \int \phi\,(f)\,\tilde{P}\,(f)\,df \tag{3.7}$$

$$\tilde{\phi}''^2 = \int (\phi\,(f) - \tilde{\phi})^2\,\tilde{P}(f)\,df \tag{3.8}$$

where $\phi(f)$ is the state relationship for the property ϕ. The time-averaged probability density function of mixture fraction, $\bar{P}(f)$, is related to $\tilde{P}(f)$, as follows:

$$\bar{P}(f) = \bar{\rho}\,\tilde{P}(f) / \rho(f) \tag{3.9}$$

Thus, time-averaged mean and mean-squared fluctuating values of any scalar property become:

$$\bar{\phi} = \int \phi\,(f)\,\bar{P}(f)\,df = \bar{\rho} \int (\phi(f) / \rho(f))\;\tilde{P}(f)\,df \tag{3.10}$$

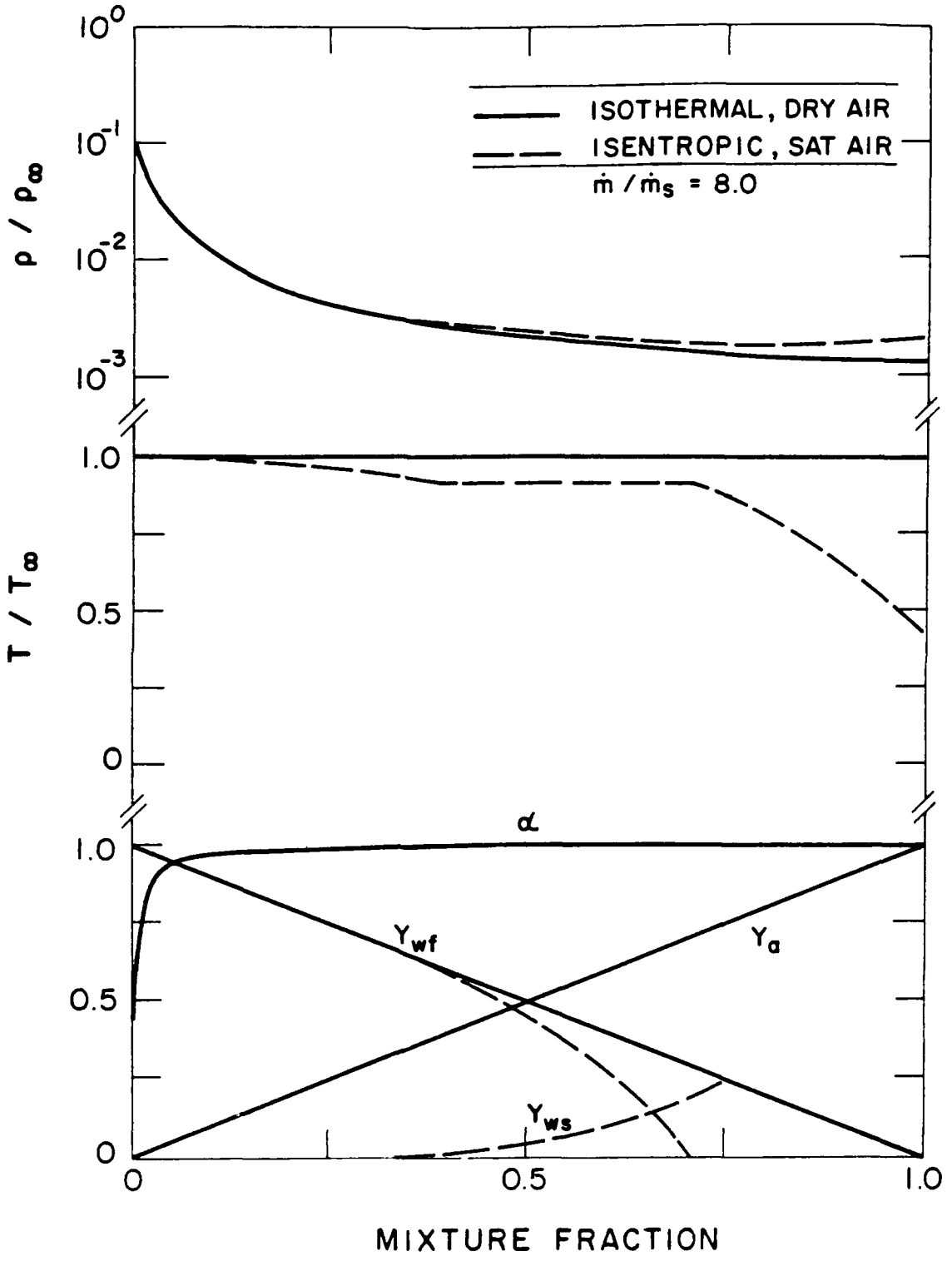

Figure 6. State relationships for air injection into water.

$$\overline{\phi}'^2 = \overline{\rho} \int ((\phi(f) - \overline{\phi})^2 / \rho(f)) \tilde{P}(f) \, df \tag{3.11}$$

The time-averaged density, $\overline{\rho}$, which is needed to solve the governing equations, is found by setting $\phi = 1$ in equation (3.10).

To complete the formulation, a functional form must be assumed for $\tilde{P}(f)$, although the specific form does not have a strong effect on predictions (Lockwood & Naguib, 1975). Any two parameter distribution can be used, within the present level of closure, since its two unknown parameters can be found by noting:

$$\tilde{f} = \int f \tilde{P}(f) \, df \tag{3.12}$$

$$g = \int (f - \tilde{f})^2 \tilde{P}(f) \, df \tag{3.13}$$

Since $\tilde{f}$ and g are known from the solution of the governing equations, equations (3.12) and (3.13) provide two implicit expressions to solve for the two parameters of the PDF.

Formally, the state relationships of equations (3.4)-(3.7) imply that air and water never coexist at a point: either pure water or pure air is present. Thus the correct state relationship for the flow invoives Dirac delta functions at f=0 and 1, which were used in specifying initial conditions as noted earlier. As a practical matter, however, spatial resolution of all measurements considered during this study was not sufficient to resolve small dispersed-phase elements like drops and small bubbles; therefore, it is also realistic to consider heterogeneous mixtures of both phases in any realizable measuring volume for observations. Thus, a clipped-Gaussian probability density function was used during the present investigation, following Lockwood & Naguib (1975) and earlier work in this laboratory (Chen & Faeth, 1982, 1983; Jeng & Faeth, 1984). Solution of the resulting transcendental equations for the most probable value and variance of this distribution was facilitated by a table constructed by Shearer et al. (1979).

The formulation for scalar properties is actually simpler for the more correct version where the PDF of mixture fraction consists of Dirac delta functions at f = 0 and 1. This approach will be stated for completeness although it is only suitable for noncondensing and nonreacting flows. Denoting scalar properties at the jet exit, where f = 1, to be ϕ_o; and scalar properties in the ambient environment of the jet, where f = 0,

to be ϕ_∞; the various Favre-and time-averaged scalar properties using the Dirac delta function PDF become:

$$\tilde{\phi} = \phi_\infty (1 - \tilde{f}) + \phi_o \tilde{f} \tag{3.14}$$

$$\bar{\phi} = (\phi_\infty \rho_o (1 - \tilde{f}) + \phi_o \rho_\infty \tilde{f}) / (\rho_o(1 - \tilde{f}) + \rho_\infty \tilde{f}) \tag{3.15}$$

$$\tilde{\phi}''^2 = (\phi_\infty - \phi_o)^2 \tilde{f} (1 - \tilde{f}) \tag{3.16}$$

$$\bar{\phi}^{12} = (\phi_\infty - \phi_o)^2 \bar{\rho}^2 \tilde{f} (1 - \tilde{f}) / (\rho_\infty \rho_o) \tag{3.17}$$

where

$$\bar{\rho} = \rho_o \rho_\infty / (\rho_o (1 - \tilde{f}) + \rho_\infty \tilde{f}) \tag{3.18}$$

In this case, mean and fluctuating quantities are fully prescribed by $\tilde{f}$ and the governing equation for g does not have to be solved. In addition to $\bar{\rho}$, which is required to solve equation (3.2), time-averaged void fractions are an important scalar property to be tested using present measurements. Noting that $\alpha_o = 1$ and $\alpha_\infty = 0$, time-averaged mean and fluctuating void fractions can be found from equations (3.15) and (3.17) as follows:

$$\bar{\alpha} = \bar{\rho} \tilde{f} / \rho_o \tag{3.19}$$

$$\bar{\alpha}'^2 = \bar{\rho}^2 \tilde{f} (1 - \tilde{f}) / (\rho_o \rho_\infty) \tag{3.20}$$

In these equations state o should be replaced by state e if the effective-adapted-jet approximation is used. Use of either the clipped Gaussian or double delta function PDF's gave nearly the same results; thus the latter is preferred for simplicity for noncondensing flows.

3.6 Computations

Equations (3.2) were integrated using a modified version of the GENMIX algorithm due to Spalding (1977). The large density variations of the present multiphase flows required a finer numerical grid than is needed for single-phase flows. Results reported in the following used 360 cross-stream grid nodes, with streamwise

step sizes chosen to be less than 0.2 percent of the current flow width, or an entrainment increase of less than 0.2 percent, whichever was limiting. Doubling the number of nodes in the mesh resulted in less than a 1 percent variation of flow properties; therefore, numerical closure was adequate, particularly in view of the other uncertainties of the analysis.

Sensitivity analysis was performed to find the influence of initial conditions on computed flow properties. Results for round jets are summarized in Table 4. Changes of 100 percent for k_e, ε_e, U_{ce} and Re have a negligible effect on computed results. Similar changes of d_e and Ri have a larger effect, however, uncertainties of these quantities are much less than 100 percent.

Table 4 Study of Sensitivity to Input Parameters

Input Parameter	Output Parameter[a]		
	$\bar{\alpha}_c$	$r_{0.5}$[b]	C_e
k_e	0.2	-1.2	-1.5
ε_e	-0.1	0.1	-0.1
u_{ce}	0.0	0.0	0.0
d_e	6.9	14.5	10.1
Re	0.1	-0.1	0.1
Ri	-5.8	-4.6	17.3

[a] Maximum increase (percent) of output parameter for round jets at x/d = 80 for a 100 percent increase of the input parameter.

[b] Radial distance were $\bar{\alpha}$ = 0.5.

4. Results and Discussion

4.1 Flow Definition

Flow Visualization. Results of flow visualization for the round jets are discussed by Loth & Faeth (1987) and Loth (1988). Motion pictures of the flow (at roughly 1000 pictures/s) gave evidence of large-scale unsteadiness for $\dot{m}/\dot{m}_s$ = 0.6 and 1.0, similar to the observations of others (Kerney et al., 1972; Weimer et al., 1973; Chan, 1974; Cho et al, 1987; Chun & Sonin, 1984; Lambier & Chow, 1984; Simpson & Chan, 1982). This involved random fluctuations of gas release (ca. 10-20/s) producing mushroom-like gas structures near the exit and the sudden appearance (ca. 1 ms) of gas below the passage exit. This behavior was similar to the pulsitile release of gas near the source of strongly-buoyant single-phase plumes. The frequency of appearance of large-scale disturbances decreased with increasing $\dot{m}/\dot{m}_s$ for underexpanded jets. Only occasional disturbances (typically 2-3/s) were observed for $\dot{m}/\dot{m}_s$ = 8, lasting only a few ms. They appear to be similar to the "reverse shocks" mentioned by Surin et al. (1983) and are associated with the external-expansion region, possibly involving interactions between shock-waves and other gas-dynamic phenomena and the motion of gas-liquid interfaces. Plenum pressure fluctuations due to these disturbances decreased monotonically with increasing injector mass flow rates, e.g., maximum plenum pressure fluctuations were 1.2 and 0.2 percent at $\dot{m}/\dot{m}_s$ of 0.6 and 8. The use of screens at the passage exit, and various injector exit configurations, injector angles (ranging from horizontal to vertically upward), liquid depths, plenum sizes and wave-damping methods, had no observable influence on the character of the large-scale unsteady disturbances. On the other hand, even low levels of liquid coflow stabilized the disturbances appreciably.

Results for the plane jets were somewhat similar to the round jets. High-speed motion pictures (at roughly 1000 pictures per second) indicated rapid lateral growth of the void-containing region of the flow. Innate unsteadiness was also observed but to a lesser degree than for the round jets. Similar to the round jets, global unsteadiness of the plane jets was reduced as the underexpansion ratio increased. For adapted flow, the disturbances were large enough so that a frequency of 5.7 Hz could be measured, however, at higher underexpansion ratios the disturbances were not sufficiently defined to judge their frequency. Since the exit of the plane jet did not protrude into the flow, no reverse flow was observed. However, preliminary tests with a protruding plane jet, having no sidewalls in the multiphase region, did produce large random disturbances and reverse flow.

Typical photographs of the appearance of the plane jet appear in Fig. 7. Figure 7A is a flash photograph for air into water while Figs. 7B and C are shadowgraphs for air into air and water - all for $\dot{m}/\dot{m}_s = 3.0$. The photograph for air into water shows the presence of a series of oval-shaped lobes extending some distance into the flow which is reminiscent of the deflection of the mixing layer for underexpanded gas jets in gases, see (Chuech et al., 1988) or Fig. 7B. Similarly, comparing Figs. 7B and C indicates are rather similar wave structure for injection of air into air and water, at least through the first lobe (or shock cell). This provides direct proof that a shock-wave-containing external-expansion region is present for underexpanded gas jets in liquids. The core of the first cell appears to be clear of drops although it is surrounded by a multiphase mixing layer. At the end of the first lobe, however, a drop-containing region is observed adjacent to the core - eminating more or less from the region where the mixing layer makes its closest approach to the plane of symmetry. The presence of drops in the core region tends to obscure the subsequent lobes but results in Fig. 7A suggest that this multiphase gas dynamic region extends some distance from the jet exit.

Static Pressures. The nature of the external expansion region for underexpanded gas jets in liquids can be seen more quantitatively from the static pressure measurements. Static pressures along the axis of round jets, for $\dot{m}/\dot{m}_s \geq 1.0$, are illustrated in Fig. 8. Results are shown for injection into both air and water, from the same 11.0 mm diameter passage. The results for injection into air are very similar to the findings of Chuech et al. (1988) for underexpanded fully-developed pipe flows in still air. Static pressures along the ais exhibit a decaying oscillatory behavior due to the presence of shock cells that eventually decay away as the mixing layers near the edge of the flow reach the axis. The static pressure variations along the axis for injection of air into water are similar to those observed for injection of air into air, at least for the first few shock cells. Notably, Surin et al. (1983) observed similar agreement of oscillatory dynamic pressure variations along the axis of underexpanded gas jets in gases and liquids. This confirms that a shock-wave-containing external-expansion region is present for underexpanded gas jets in liquids. The main difference between the static pressure records for underexpanded air jets in air and in water is that the external-expansion region decays more rapidly for injection into water. This behavior is expected since turbulent mixing is more rapid when a low-density material is injected into a high-density environment (Chen & Faeth, 1982, 1983; Faeth, 1987).

Static pressures along the axis of the plane jets are illustrated in Fig. 9 for $\dot{m}/\dot{m}_s \geq 1.0$ for injection into both air and water. The results are generally similar to the findings for the round jets: the static pressure variation in the external-expansion region

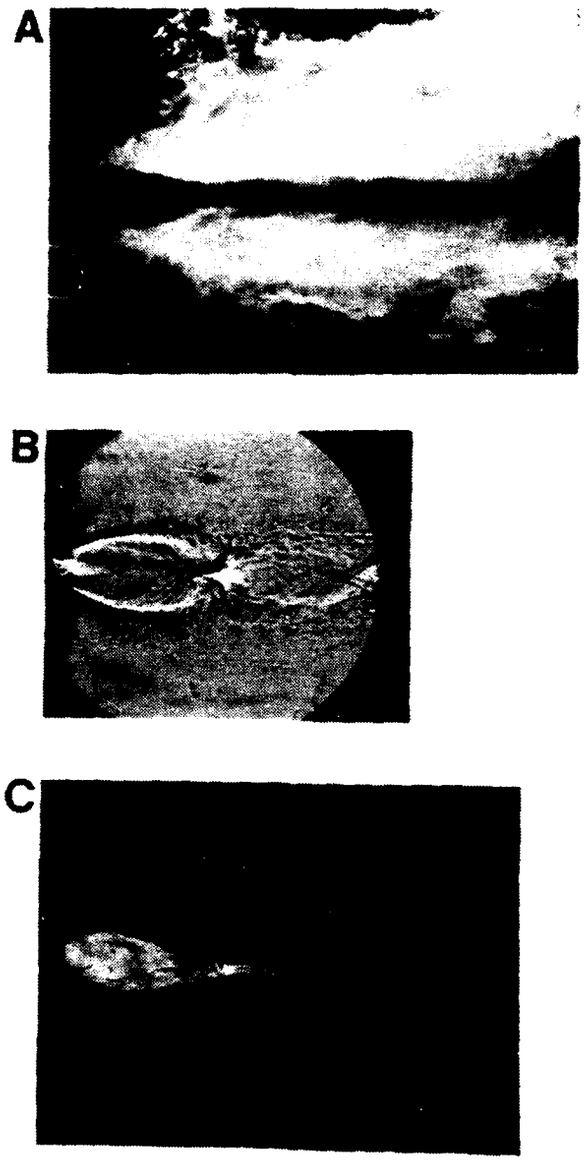

Figure 7. Plane injector at m/m_s = 3.0: A) flash photograph of air into water, B) shadowgraph of air into air, C) shadowgraph of air into water.

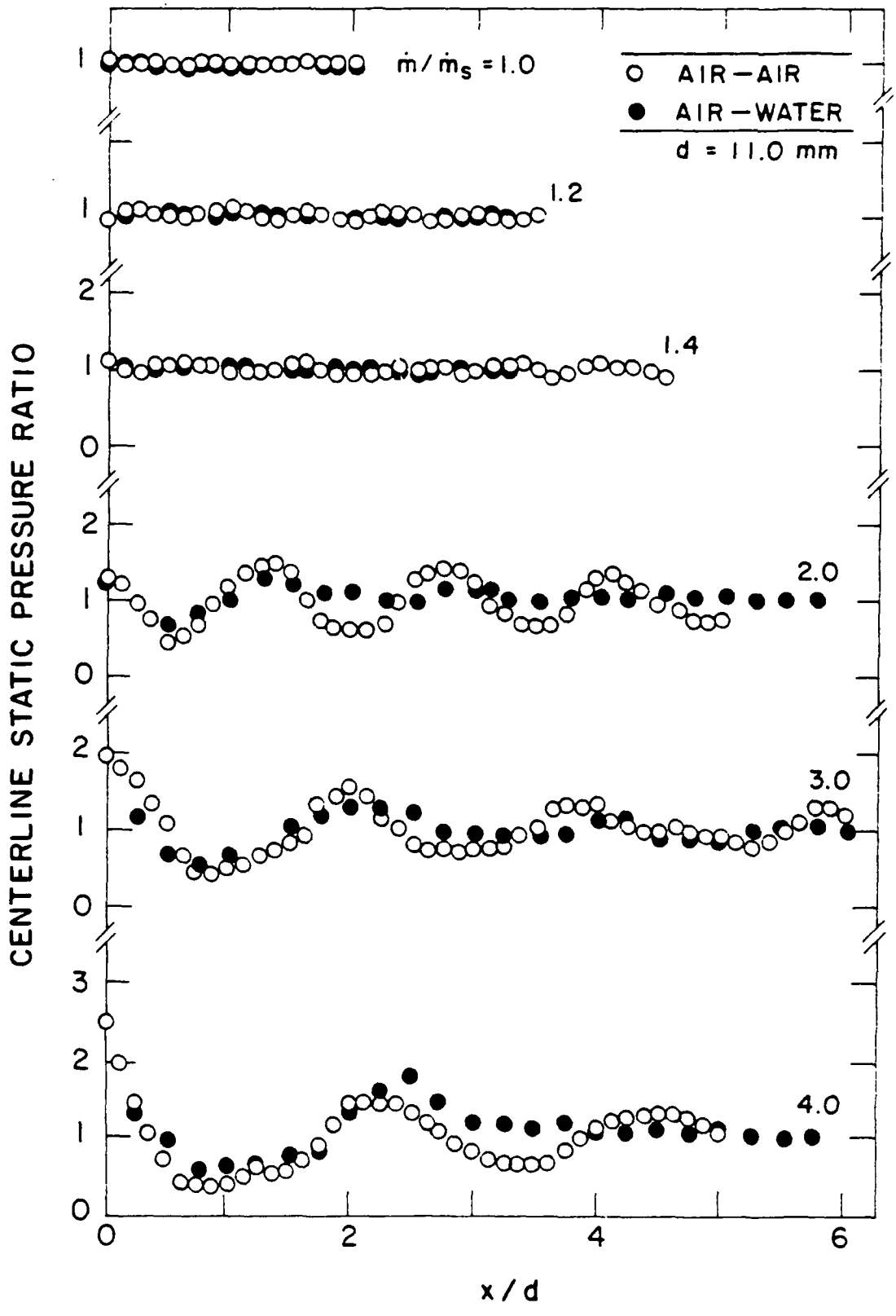

Figure 8. Static pressure distribution along axis for round jets.

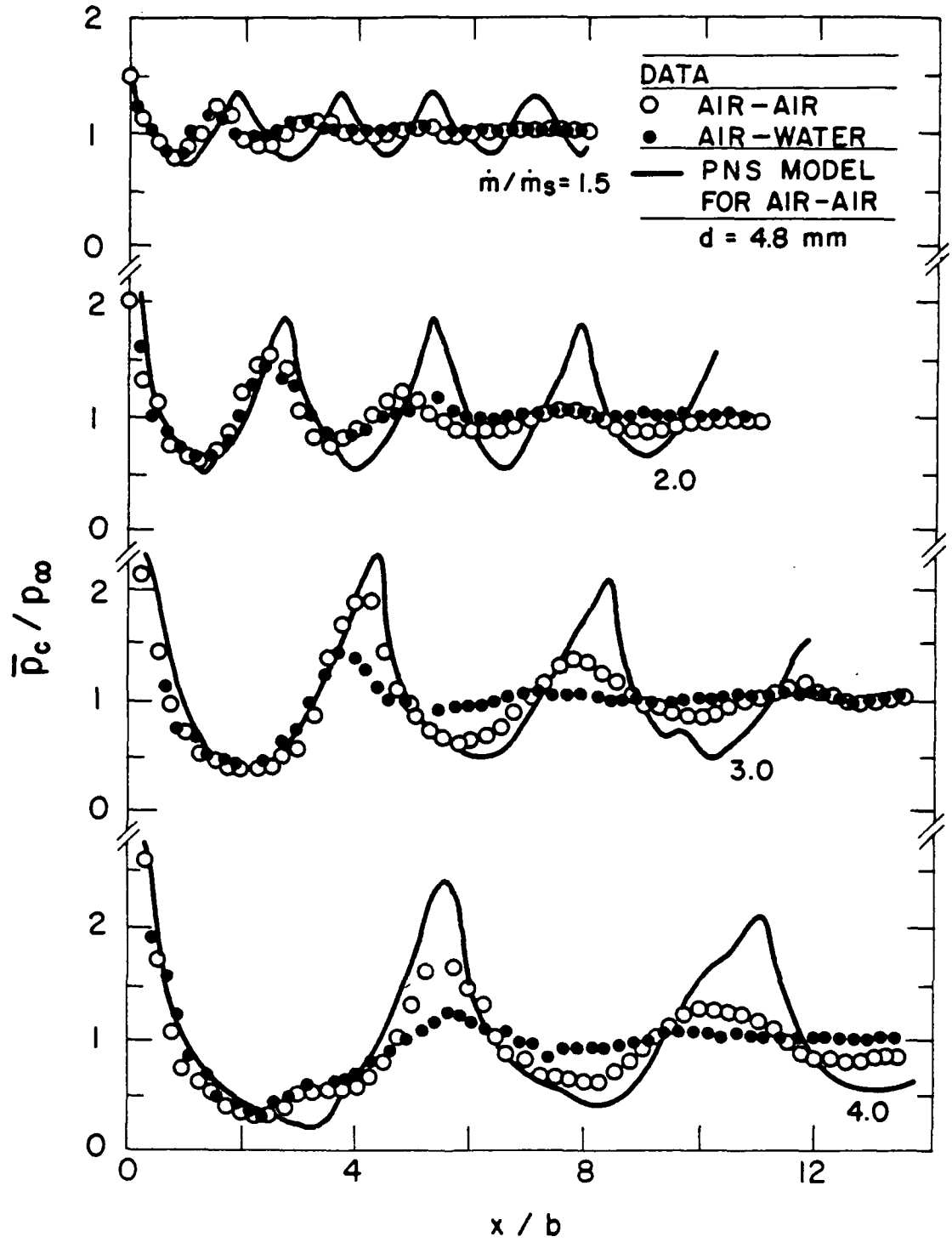

Figure 9. Static pressure distribution along axis for plane jets.

is similar for injection into air and water although the latter decays more rapidly. Computations using a parabolized Navier-Stokes method described by Chuech (1987) and Cheuch et al. (1988) are also shown on the plot for comparison with measured properties of air jets in air. The comparison between predictions and measurements is not very good, largely due to the presence of acoustic feedback which is discussed next.

Acoustic Feedback. Another important feature of the passage exit condition is the presence of acoustic feedback within the shock-cell pattern. Acoustic feedback arises as a result of pressure disturbances traveling upstream near the edge of the jet, reflecting from the surfaces near the exit plane of the nozzle and resonating at a particular frequency. The tuning condition is set by the sound wave speed of the ambient fluid and an acoustic reflection distance from the jet exit to some downstream position of the external expansion region, associated with one of the shock cells. Sherman et al. (1976) have reported substantially increased mixing due to acoustic feedback for underexpanded air jets in air, with dominant feedback frequencies approximately proportional to the sonic speed divided by the first or second shock-cell length.

Measurements with a hydrophone at a radial/lateral position of six exit widths from the centerline and six exit widths downstream were completed for the 4.9 mm round injector and the 4.8 mm plane injector, for air injected both into air and into water. Power spectral densities of the acoustic signal are plotted as a function of frequency in Figs. 10 and 11 for the round and plane jets, respectively. Measurements were made for frequencies of up to 62 kHz (the approximate Strouhal number), with significant signal content found in the 1-25 kHz regime. Little evidence of acoustic feedback for the round jet into still air was observed, except for a resonance at 23 kHz for a mass flow ratio of two. This is not surprising since the injector was protruding and provided little surface area to reflect acoustic waves. For injection into still water, signal levels are typically lower at high frequencies, ca. 5-25 kHz, and no evidence of acoustic feedback is observed. This behavior may be due to the higher acoustic velocity of water than air, which would vastly modify tuning conditions for acoustic feedback.

There is substantial evidence of acoustic feedback in Fig. 11 for all the underexpansion ratios for the plane air jet into air. Feedback peaks are especially large at mass flow ratios of two and three, with frequencies corresponding to acoustic reflection distances of several exit widths. The flat surface along the exit plane is probably responsible for this dramatic increase in acoustic feedback, since it provides a reflecting surface for acoustic disturbances. These strong effects of acoustic feedback

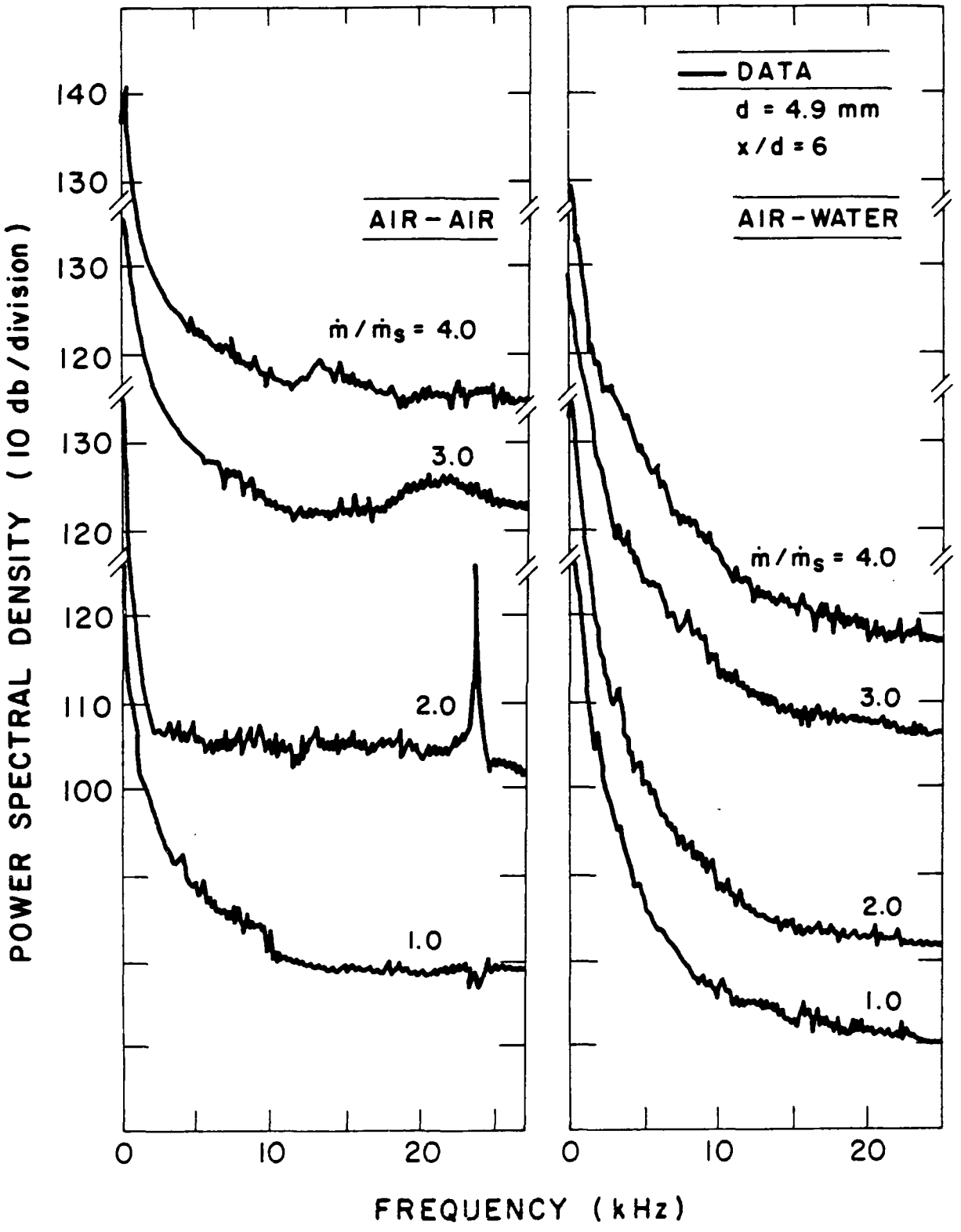

Figure 10. Power spectral density of acoustic signal for round jets.

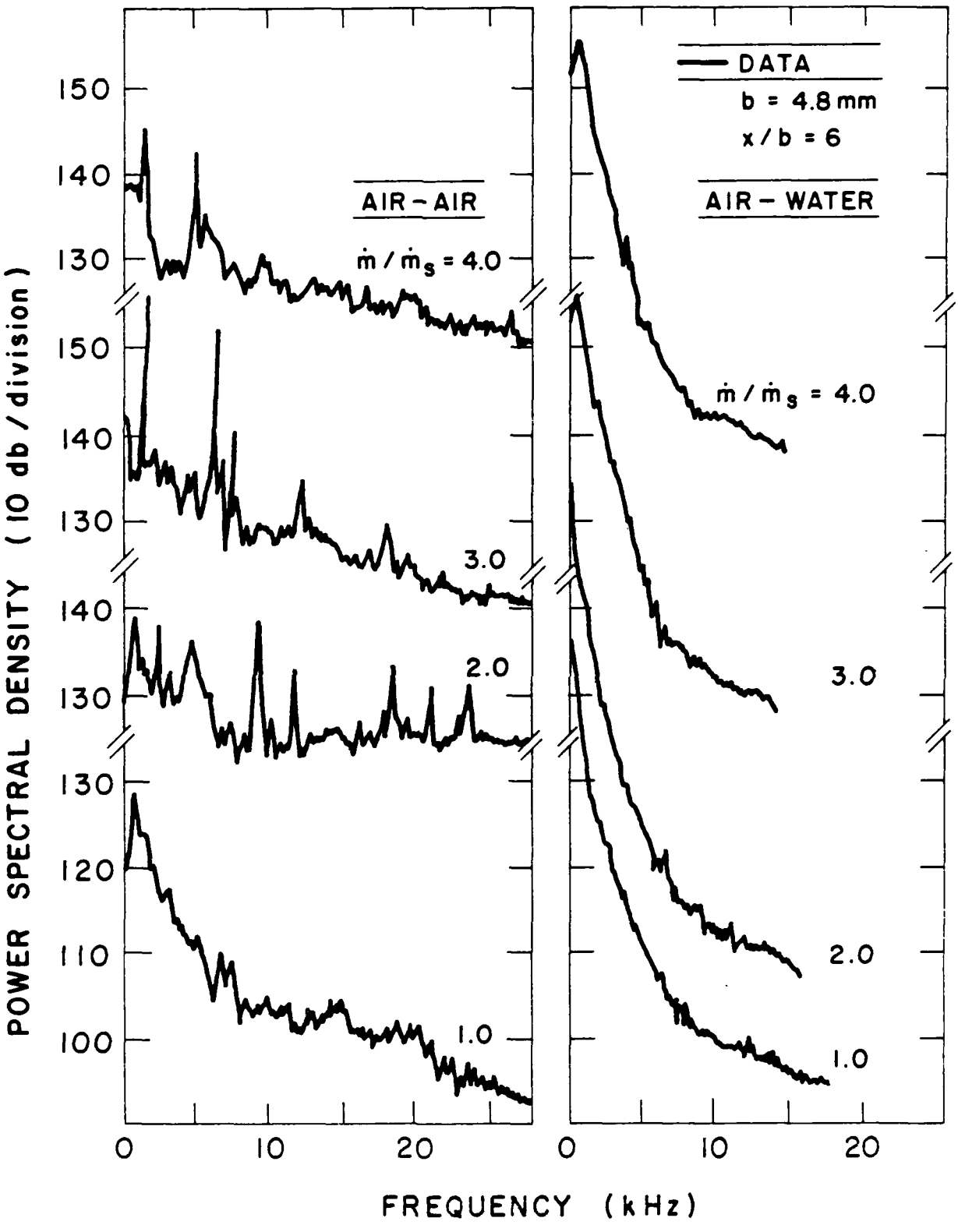

Figure 11. Power spectral density of acoustic signal for plane jets.

probably explain the more rapid decay of static pressures than predicted in Fig. 9 for underexpanded air jets in air. Similar to the round jet, however, injection into water yields lower acoustic levels at the high frequencies, ca. 5-25 kHz, and no evidence of acoustic feedback. In addition to effects of the different acoustic velocities of water and air, the presence of bubbles in the multiphase flow may also damp pressure waves, as reported by Borisov (1983). These acoustic measurements indicate that the plane jet may exhibit enhanced mixing in comparison to the round injector due to the presence of a reflective surface near the jet exit, similar to the findings of Sherman et al. (1976). Present measurements also indicate that acoustic feedback is eliminated when water is the ambient medium, even when reflective surfaces are present.

4.2 Flow Structure

4.2.1 Round Jets

Initial Conditions. Measurements of mean and fluctuating velocities at the exit of the round jets, for all underexpansion ratios considered here, are reported by Loth & Faeth (1987). As noted earlier, these results confirmed that the flows were essentially fully-developed pipe flows at the jet exit.

Void Fractions. Measurements and predictions using standard initial conditions for round jets have already been discussed by Loth & Faeth (1987). These results will be revisited in the following, considering the effect of the using of mixed initial conditions and well as additional measurements of Bell et al. (1972), Carreau et al. (!985) and Tross (1974).

Time-averaged void fractions along the axis of the round jets, $\bar{\alpha}_c$ are illustrated in Fig. 12. Results shown include present measurements for d = 4.9 mm, the probe measurements of Tross (1974) for $\dot{m}/\dot{m}_s$ = 1.0 and 2.0, and predictions (denoted EEC model) using both standard and mixed initial conditions. The measurements of Tross (1974) are consistently lower than the present measurements in the region where they can be compared. This behavior is expected since all biases of probes tend to reduce observed void fractions (Tross, 1974). It is felt that the present nonintrusive gamma-ray absorption measurements are more reliable. The measurements show that mixing rates along the axis are progressively reduced as the underexpansion ratio is increased. This slower rate of mixing is the price that must be paid to obtain more stable injector operation by increasing $\dot{m}/\dot{m}_s$.

Predictions agree reasonably well with present measurements in Fig. 12, for $\dot{m}/\dot{m}_s \geq 2$ where effects of unsteadiness are reduced. Use of mixed initial conditions

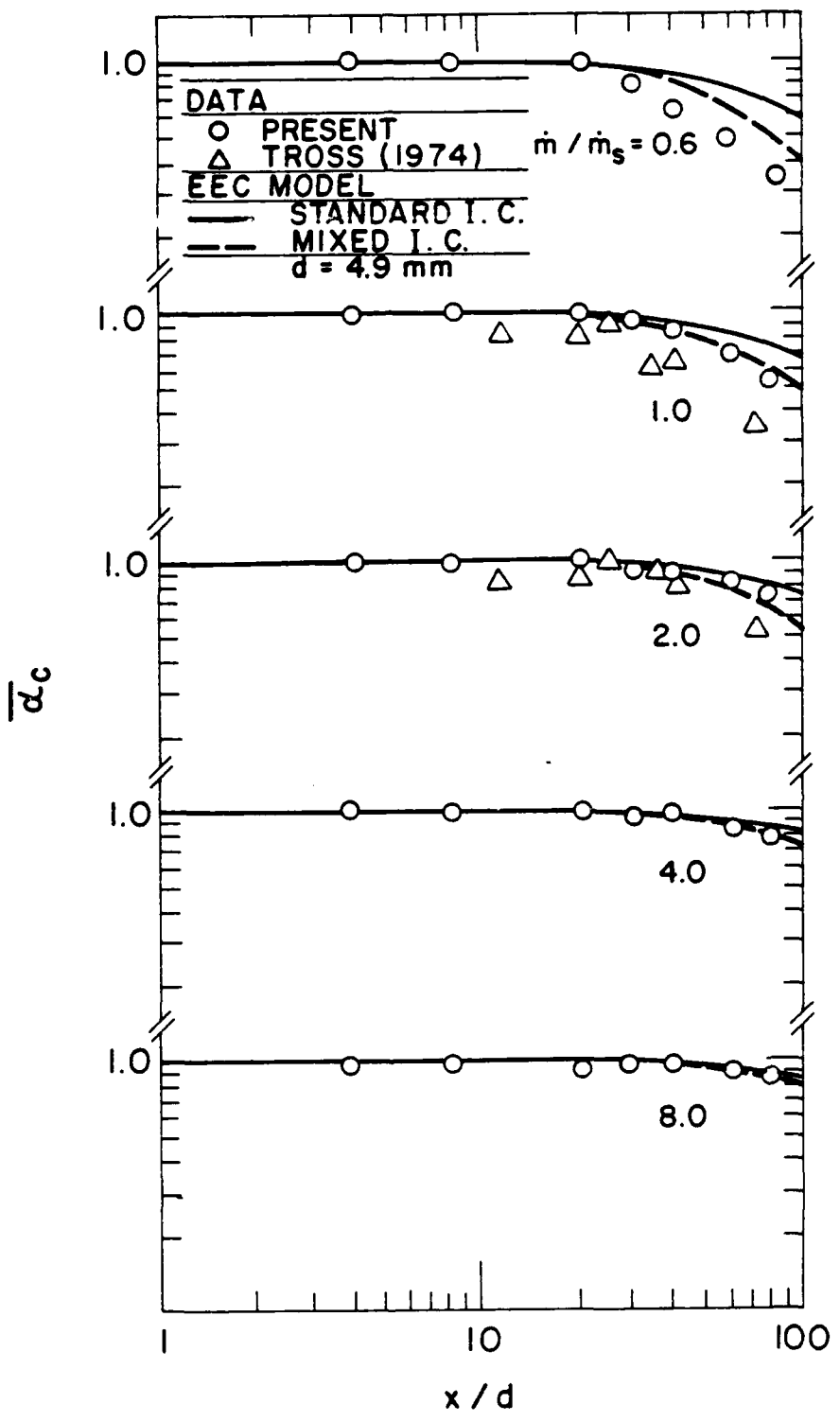

Figure 12. Time-averaged void fractions along axis of round jets.

provide somewhat better agreement with measurements than the standard initial conditions at lower values of $\dot{m}/\dot{m}_s$, however, both methods still underestimate mixing rates at $\dot{m}/\dot{m}_s = 0.6$. This deficiency cannot be due to the LHF approximation, which invariably causes mixing rates of multiphase flows to be overestimated (Faeth, 1987) while the effective-adapted-jet approximation is not used at $\dot{m}/\dot{m}_s = 0.6$. Thus, increased large-scale unsteadiness observed at low $\dot{m}/\dot{m}_s$ is probably responsible for enhanced mixing exhibited by the measurements.

Measured and predicted radial distributions of time-averaged void fractions, $\bar{\alpha}$, are illustrated in Figs. 13-17 for $\dot{m}/\dot{m}_s = 0.6$, 1.0, 2.0, 4.0 and 8.0. The results are plotted as a function of r/x, which is the radial similarity variable for fully-developed single-phase turbulent jets, so that the actual width of the flow can be seen. In addition to the present data for 4.9 and 11.0 mm diameter passages, probe measurements from Tross (1974) are also shown for $\dot{m}/\dot{m}_s = 1.0$ and 2.0. Similar to the measurements along the axis, the measurements of Tross (1974) are generally lower than present measurements, probably due to probe biases.

The most striking feature of the measurements illustrated in Figs. 13-17 is the unusual width of the void fraction profiles. This is expected near the passage exit when results are plotted as a function of r/x. Furthermore, at x/d = 4 and $\dot{m}/\dot{m}_s = 2.0$ and 4.0, there is a bulge in the void fraction distribution near the edge of the flow which is probably associated with the presence of the external-expansion region at this position (see Fig. 8). Nevertheless, flow widths remain unusually large even at x/d = 80 where the flow might be expected to approach the properties of fully-developed jets, e.g., the edge of the gas-containing region is at r/x ~ 0.3 at x/d = 80, which is nearly twice the width observed for properties in fully-developed single-phase jets (Wygmanski & Fiedler, 1969). The main reason for this behavior is that void fraction is an unusually sensitive indicator of the mixing level of the flow at low void fractions (see Fig. 6). Recall that when the mixture fraction $f << \rho_a/\rho_w$, the density ratio of air and water, the relationship between void fraction and mixture fraction becomes (equation (3.6)):

$$\alpha \approx \rho_w f / \rho_a \tag{4.1}$$

For present test conditions $\rho_w / \rho_a \sim 850$; therefore, α is still significant even when f is much smaller than values of mixing levels that would normally be associated with the edge of a jet.

In view of the sensitivity of void fractions to mixing levels (mixture fraction), the comparison between predictions and measurements in Fig. 13-17 is encouraging, in

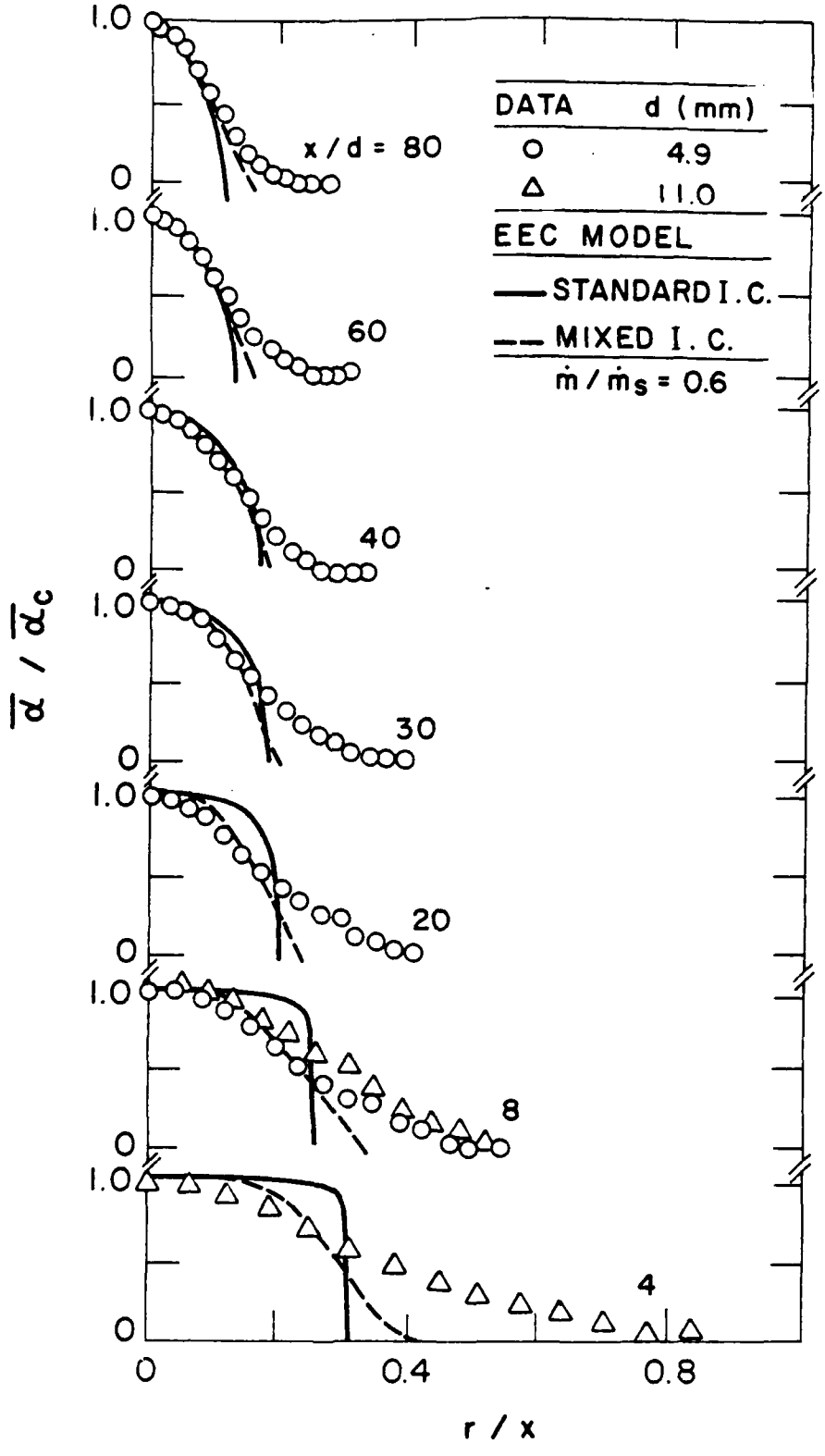

Figure 13. Time-averaged void fractions of round jets for $\dot{m}/\dot{m}_s = 0.6$.

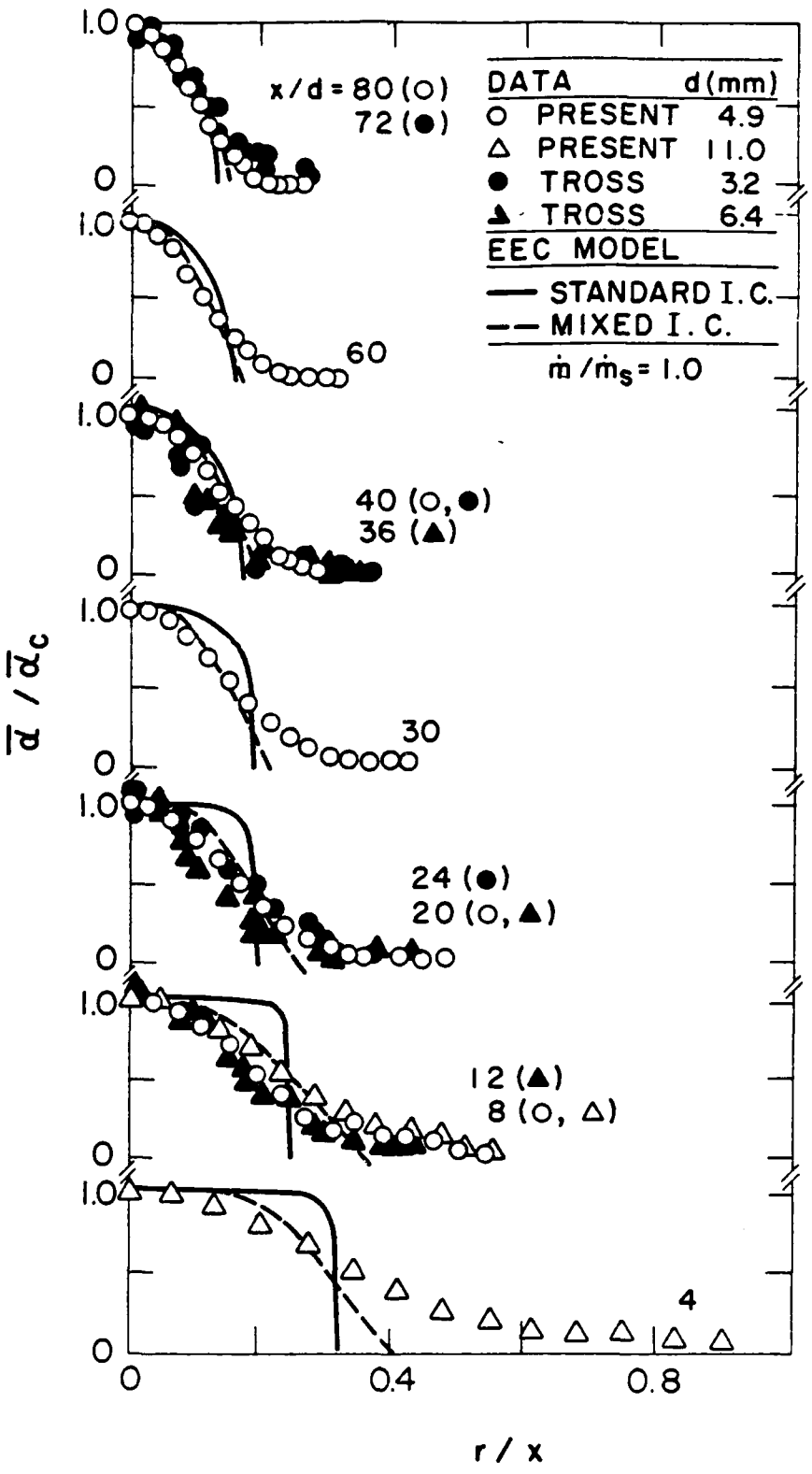

Figure 14. Time-averaged void fractions of round jets for $\dot{m}/\dot{m}_s$ = 1.0.

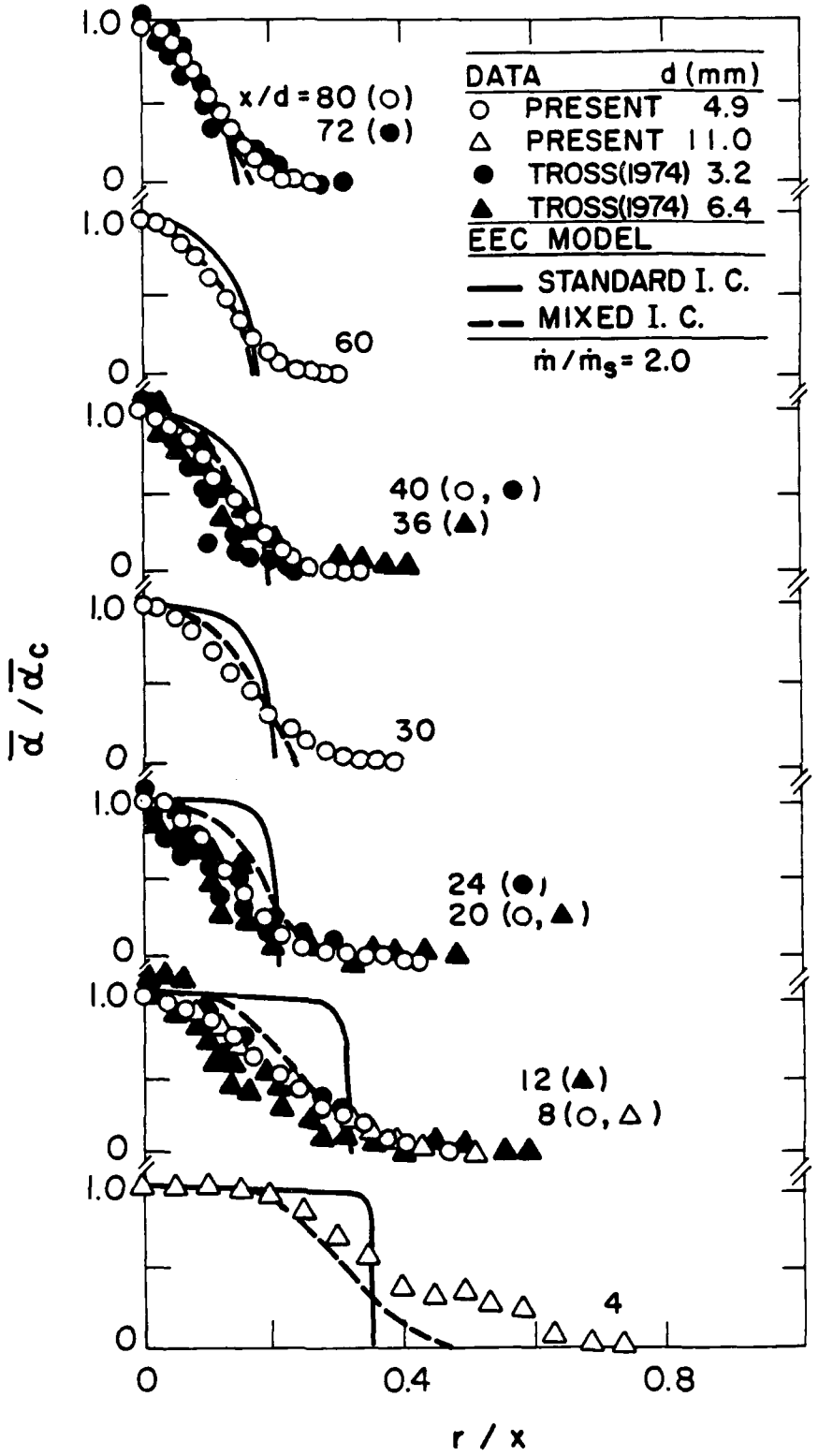

Figure 15. Time-averaged void fractions of round jets for $\dot{m}/\dot{m}_s = 2.0$.

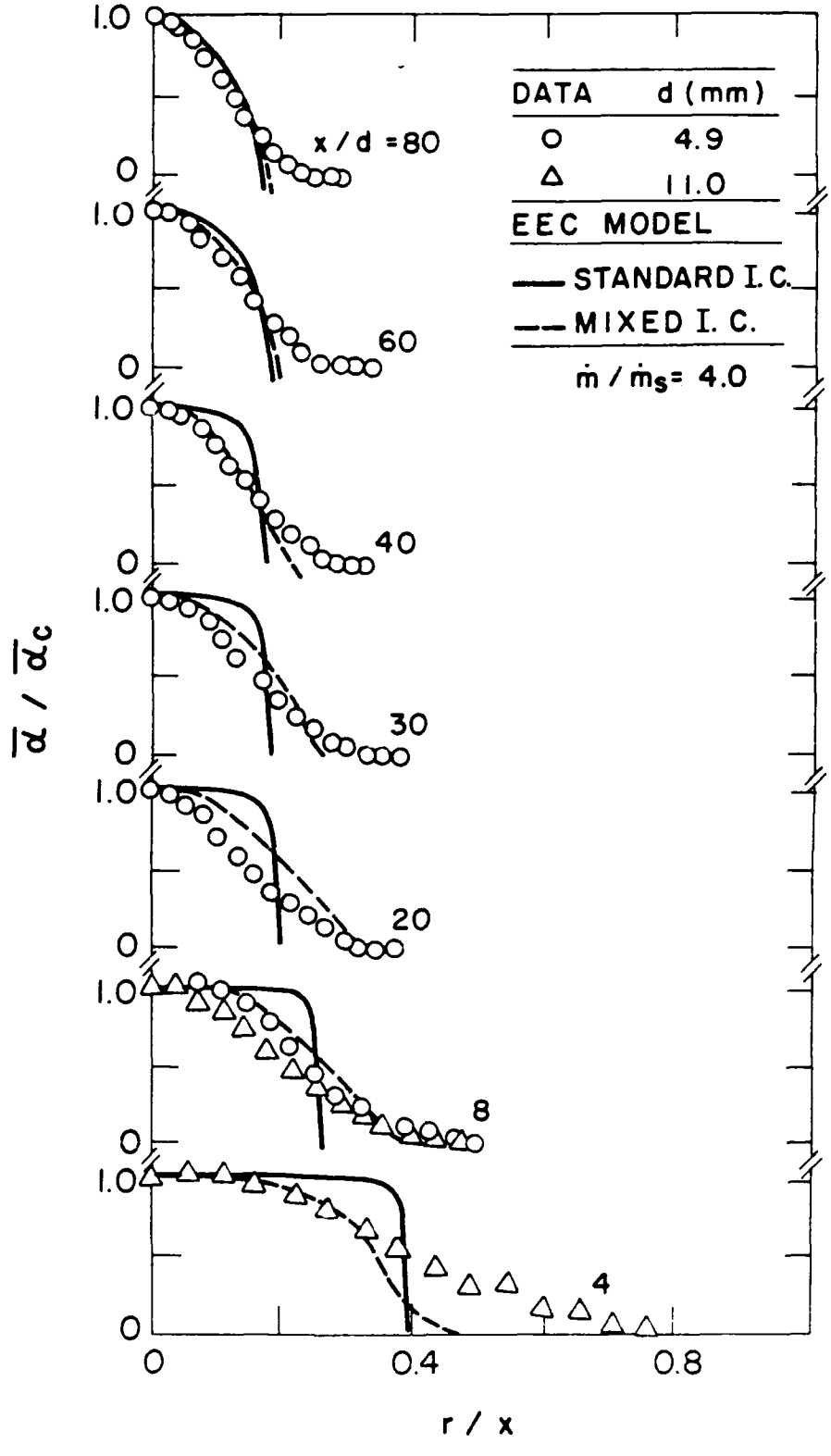

Figure 16. Time-averaged void fractions of round jets for $\dot{m}/\dot{m}_s$ = 4.0.

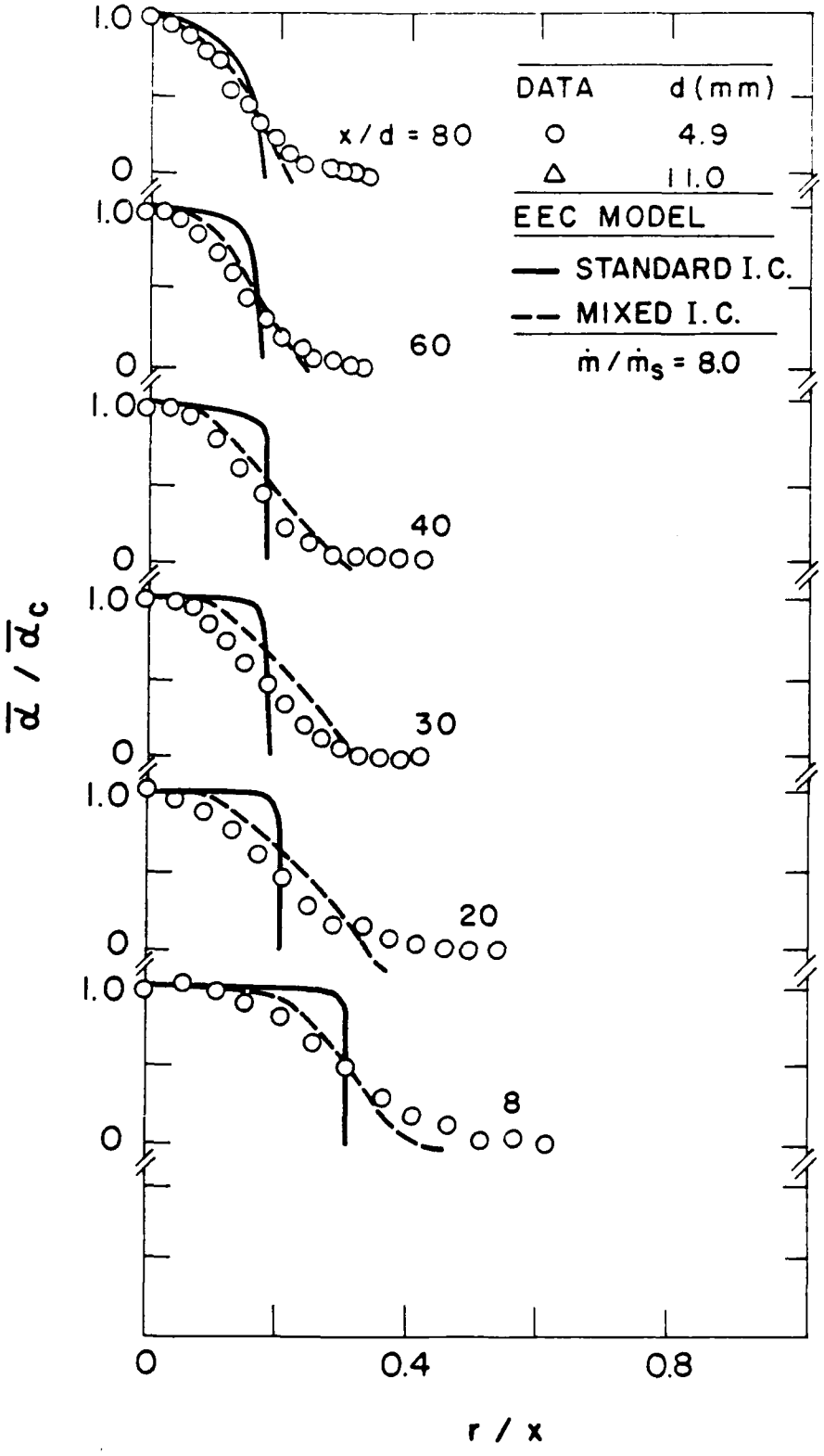

Figure 17. Time-averaged void fractions of round jets for $\dot{m}/\dot{m}_s = 8.0$.

the sense that predicted characteristic flow widths tend to scale with the measurements as x/d and $\dot{m}/\dot{m}_s$ vary. However, the evolution of the profiles from the distribution prescribed at the jet exit is relatively slow and profiles using standard initial conditions are far too blunt in the radial direction, particularly near the passage exit. Use of the mixed initial conditions yields much better predictions of the shape of the profiles, particularly near the jet exit. This suggests that mixing is enhanced near the jet exit for all conditions, probably as a result of intrinsic unsteadiness. In particular, failure of the LHF approximation generally causes overestimation of flow widths (Faeth, 1987), thus, separated-flow phenomena do not provide an obvious explanation of the discrepancies between predictions and measurements seen in Figs. 13-17. Similarly, the shapes of void fraction profiles do not differ for adapted and underexpanded jets; thus, use of the effective-adapted-jet approximation is not an obvious source of the discrepancies either.

Figure 18 is an illustration of measured and predicted characteristic void-fraction-diameters, $2r_{0.5}$ (defined as twice the radius where $\bar{\alpha}/\bar{\alpha}_c = 0.5$) plotted as a function of x/d for various $\dot{m}/\dot{m}_s$. Also shown on the plot is the radius of the gas containing region, which is roughly comparable to $2r_{0.5}$, measured by Bell et al. (1972) using a passage plate having various hole diameters for an underexpansion ratio of 3.7. The results of Bell et al. (1972) are in reasonably good agreement with present measurements in view of the somewhat different definitions of characteristic diameters. The unusual width of these flows, when viewed in terms of $\bar{\alpha}$, is evident from the figure. As before, this reflects the sensitivity of void fractions to mixing levels (note that a void fraction of 0.5 corresponds to mixture fractions of roughly 0.1 percent). The characteristic void fraction diameters increase everywhere as the underexpansion ratio increases: even at x/d = 80, $2r_{0.5}$ / x ~ 0.2 for $\dot{m}/\dot{m}_s = 0.6$ and ~ 0.3 for $\dot{m}/\dot{m}_s = 8.0$. Predictions using the two initial conditions only differ near the jet exit and are in reasonably good agreement with the measurements.

Dynamic Pressures. Other flow properties exhibit more conventional characteristic flow widths than void fractions since they are less sensitive to mixing levels. This can be illustrated using measurements of dynamic pressures from Tross (1974) for conditions very similar to the present investigation. Although these measurements were obtained using probes, reasonable comparisons between the probe measurements and present nonintrusive measurements of void fractions provide some confidence in the results.

Measured and predicted dynamic pressures along the axis are illustrated in Fig. 19. The results involve two initial jet diameters, 3.2 and 6.4 mm, and $\dot{m}/\dot{m}_s = 1.0, 1.5$

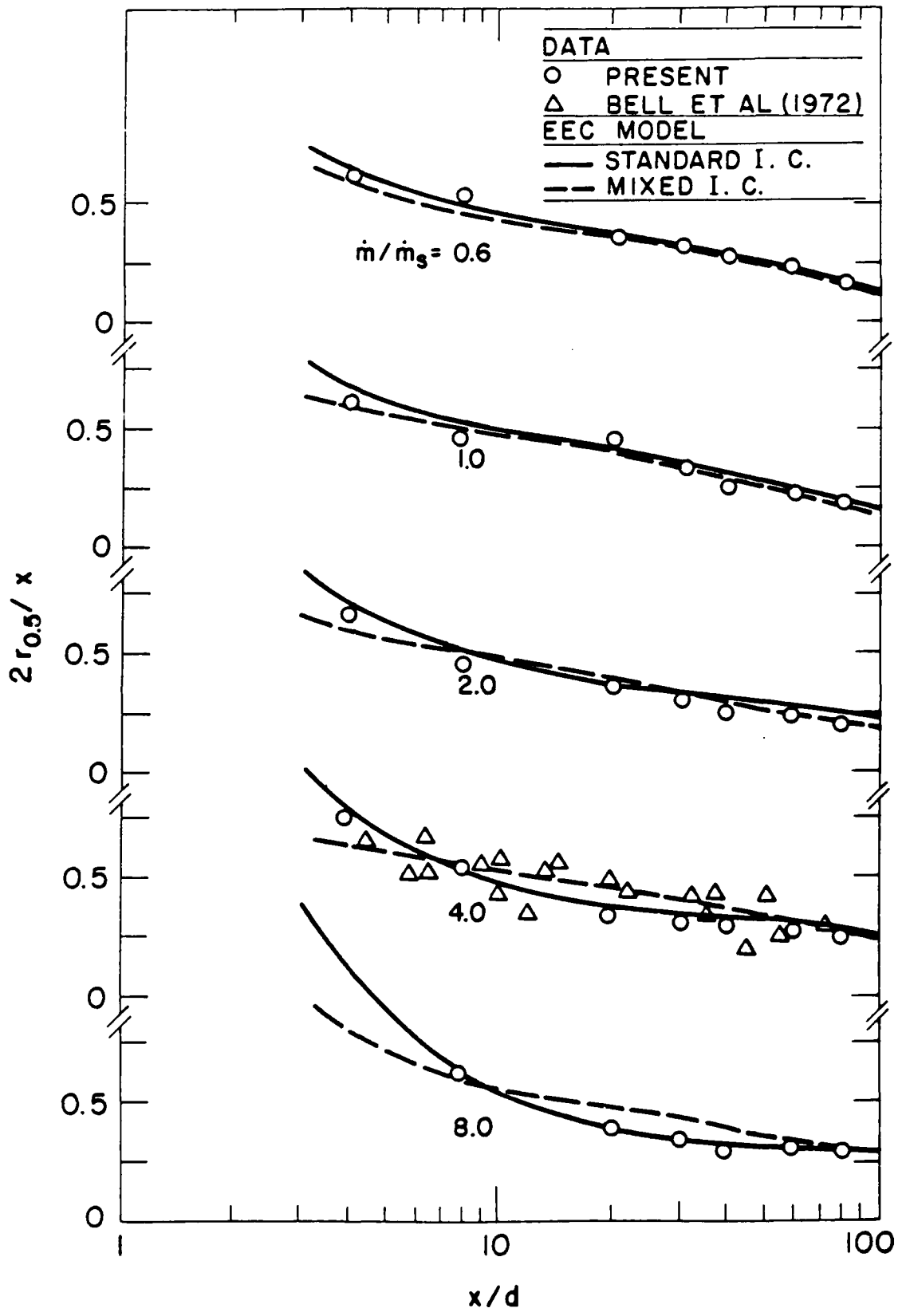

Figure 18. Streamwise variation of characteristic void-fraction diameter for round jets.

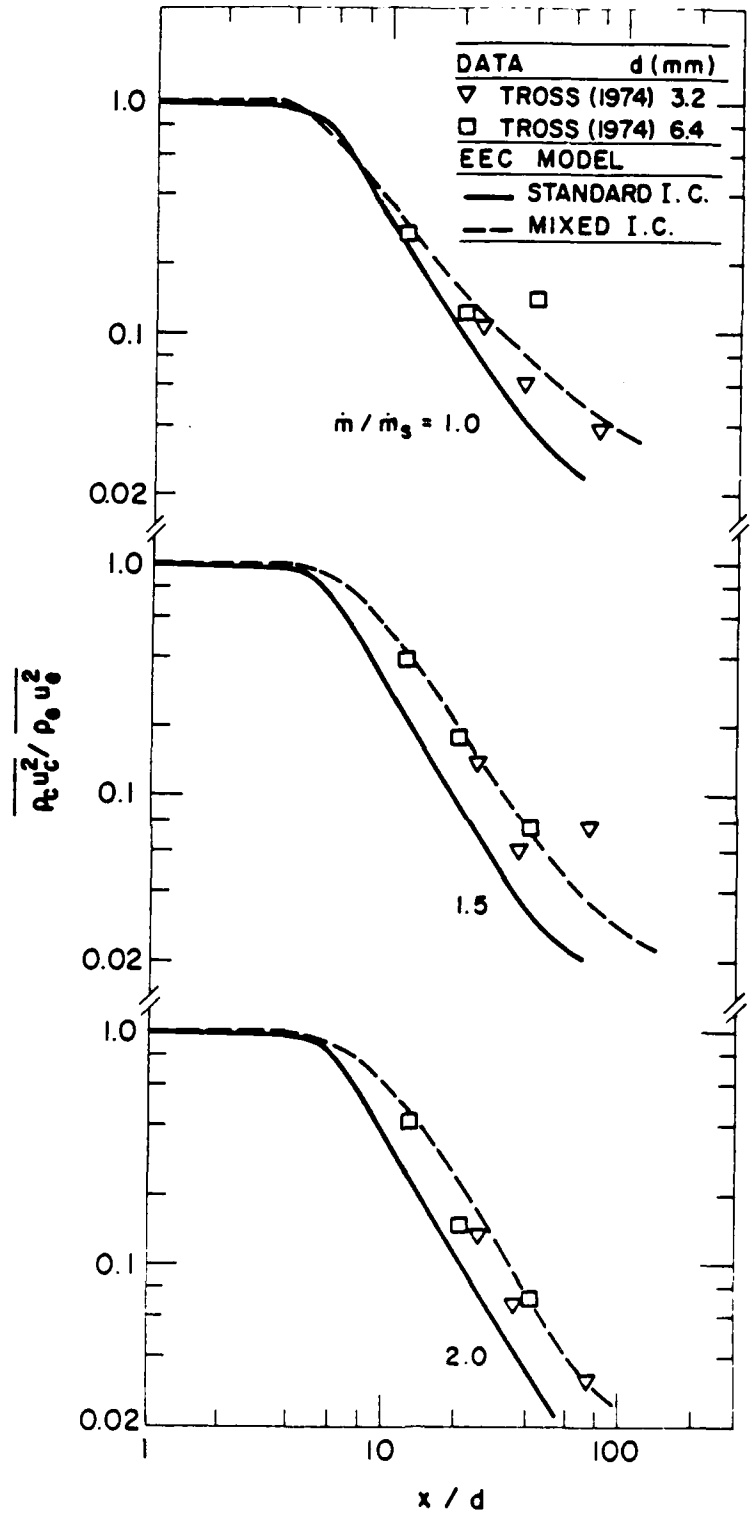

Figure 19. Streamwise variation of mean dynamic pressure for round jets.

and 2.0. Although void fractions do not increase appreciably from unity until x/d ~ 30 for these conditions (see Fig. 12), dynamic pressures begin to decrease before x/d = 10 and then exhibit a logarithmic decay typical of fully-developed single-phase jets. This difference is a result of the large density ratio of the flow, i.e., small volumes of liquid can absorb large amounts of momentum from the gas. Predictions based on the standard initial conditions tend to overestimate the rate of decay of dynamic pressures; in contrast, use of mixed initial conditions yields reasonably good agreement with the measurements - supporting the presence of unusually high mixing levels near the jet exit. An obvious defect of the predictions, however, is that use of the effective-adapted-jet approximation cannot provide information concerning dynamic pressure variations in the external-expansion region, analogous to the static pressures illustrated in Fig. 8.

Radial distributions of dynamic pressures reported by Tross (1974) are illustrated in Figs. 20-22 for $\dot{m}/\dot{m}_s$ = 1.0, 1.5 and 2.0. Predictions using standard and mixed initial conditions are also shown on the plots: there is little difference between the two predictions for these variables.

Flow widths exhibited by dynamic pressures in Figs. 20-22 are far more typical of the properties of single-phase jets than flow widths based on void fractions, e.g., the edge of the flow is at r/x ~ 0.15 for x/d = 72. Present predictions and the measurements are in good agreement for the underexpanded jets: $\dot{m}/\dot{m}_s$ = 1.5 and 2.0. Predictions indicate a narrower flow field than measured for the adapted jet (Fig. 20). This is consistent with the presence of significant effects of unsteadiness at this condition, which would be expected to enhance mixing rates.

Entrainment. Predicted and measured entrainment coefficients for the round jets, defined according to equation (2.2) are plotted in Fig. 23. Experimental results include present measurements: measurements of Bell et al. (1972) and Carreau et al. (1985) for horizontal underexpanded nitrogen jets in water, using the water overflow technique; and the empirical correlation of Ricou & Spalding (1961) for the fully-developed region of single-phase, variable-density gas jets. The present measurements and those of Carreau et al. (1985) are in excellent agreement. The earlier measurements of Bell et al. (1972), however, are more scattered and are generally higher than the rest: the reason for this difference in behavior is not known. Measured entrainment coefficients are relatively constant at small x/d but begin to increase at larger x/d, with the increase beginning sooner as $\dot{m}/\dot{m}_s$ is reduced. This is an effect of buoyancy increasing the momentum of the flow, which becomes important nearer to the jet exit as $\dot{m}/\dot{m}_s$ decreases, since this reduces the initial streamwise momentum of the flow. When effects of buoyancy are small, the entrainment coefficient remains nearly constant in the

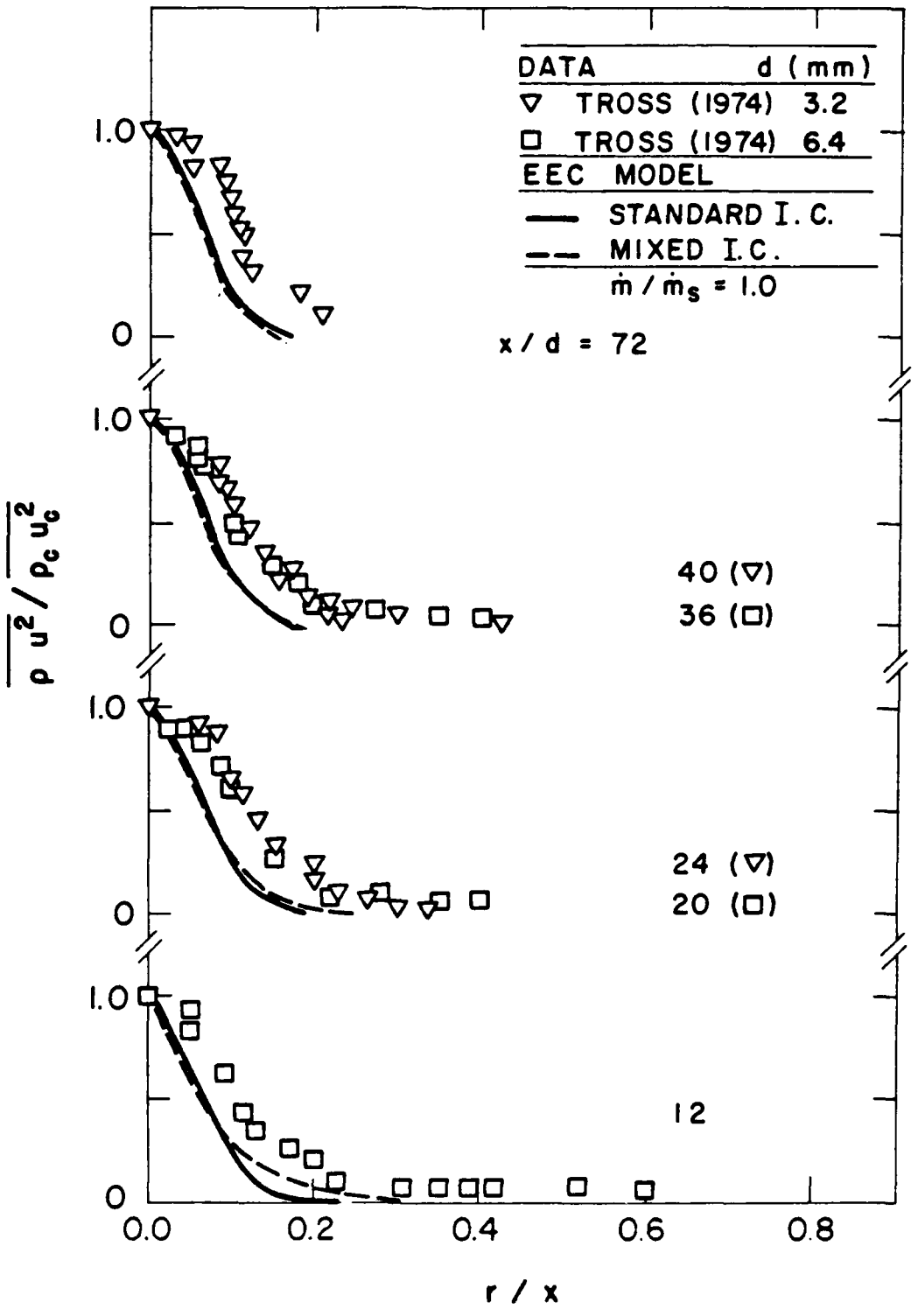

Figure 20. Mean dynamic pressures of round jets for $\dot{m}/\dot{m}_s = 1.0$.

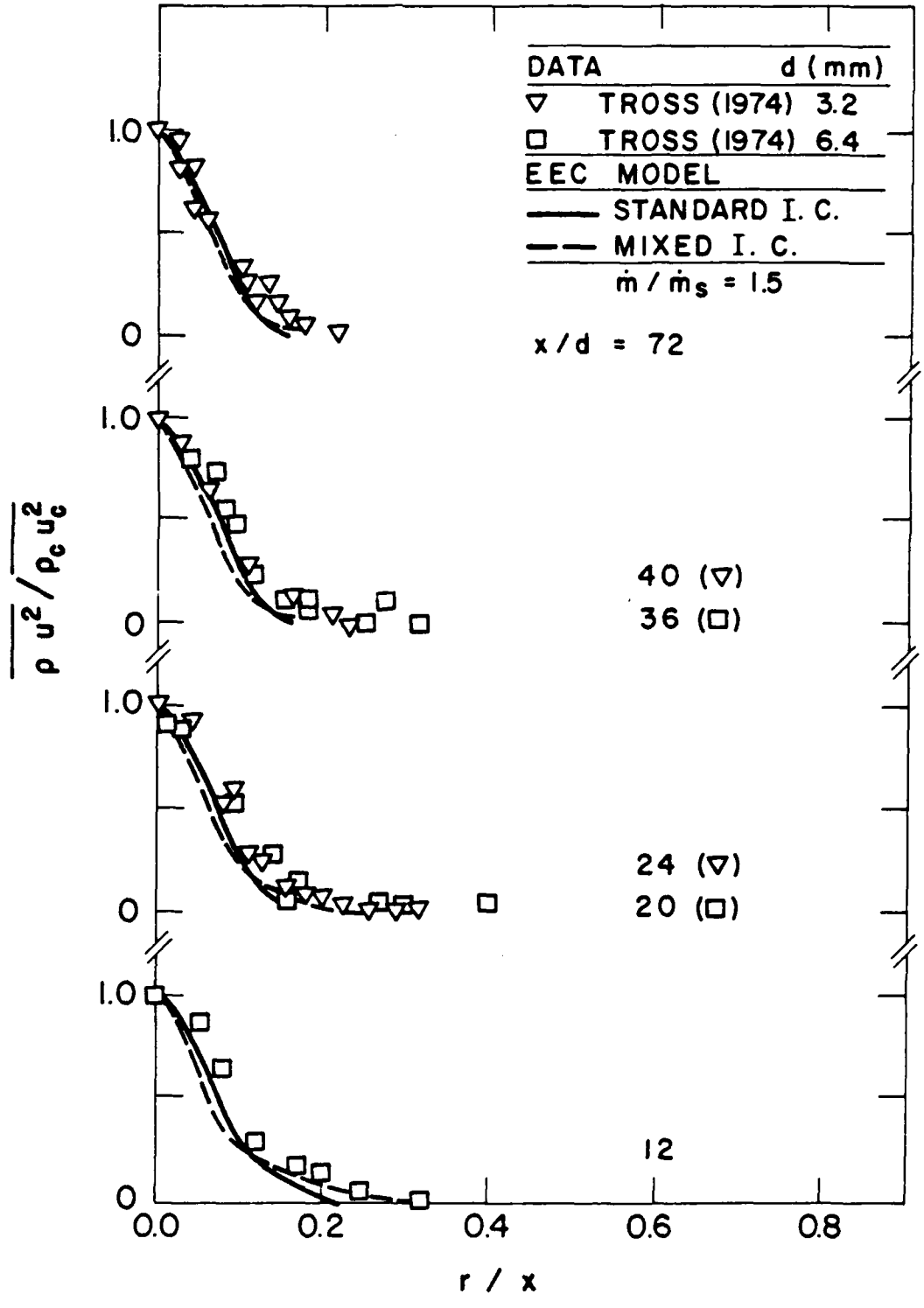

Figure 21. Mean dynamic pressures of round jets for $\dot{m}/\dot{m}_s = 1.5$.

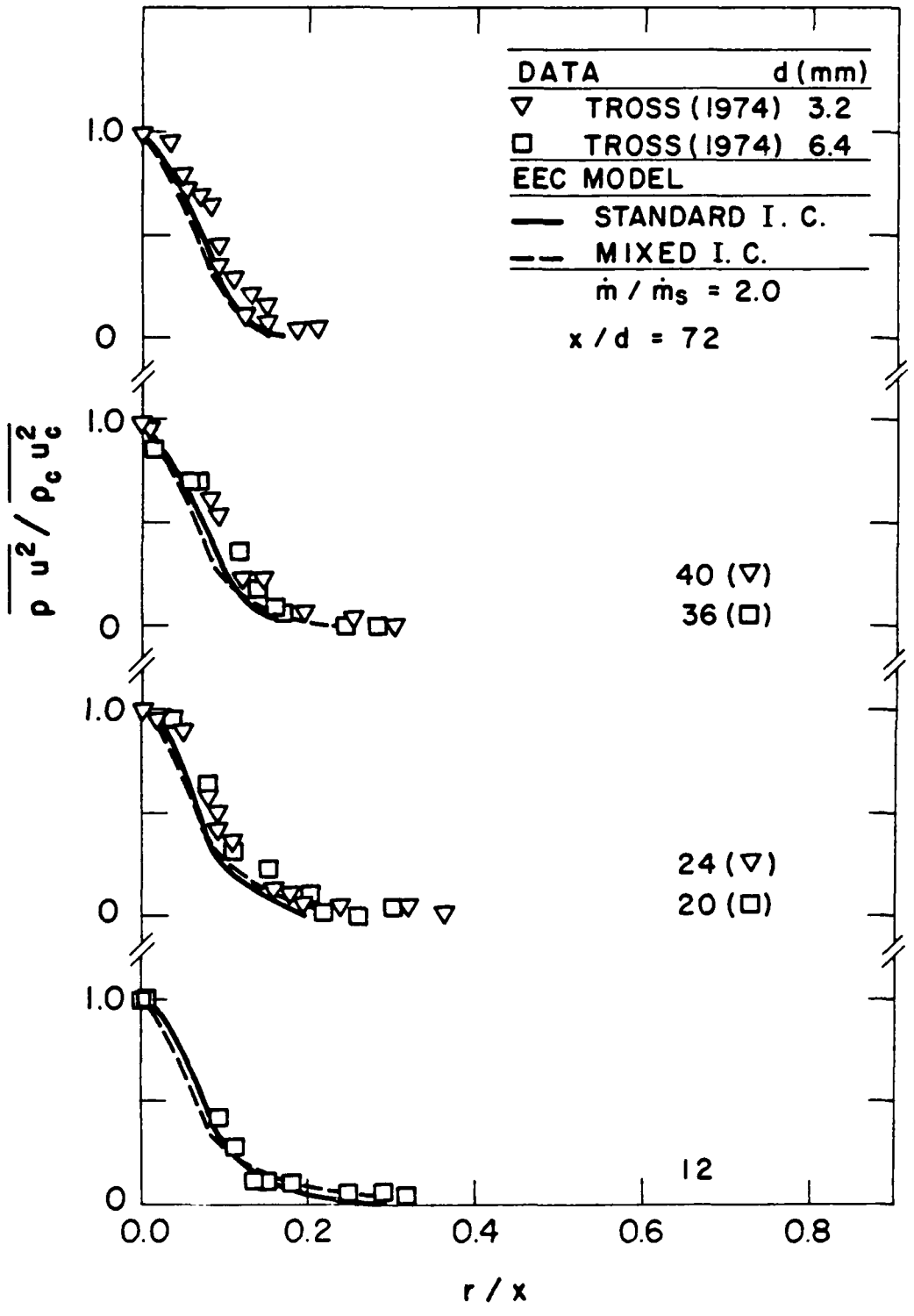

Figure 22. Mean dynamic pressures of round jets for $\dot{m}/\dot{m}_s = 2.0$.

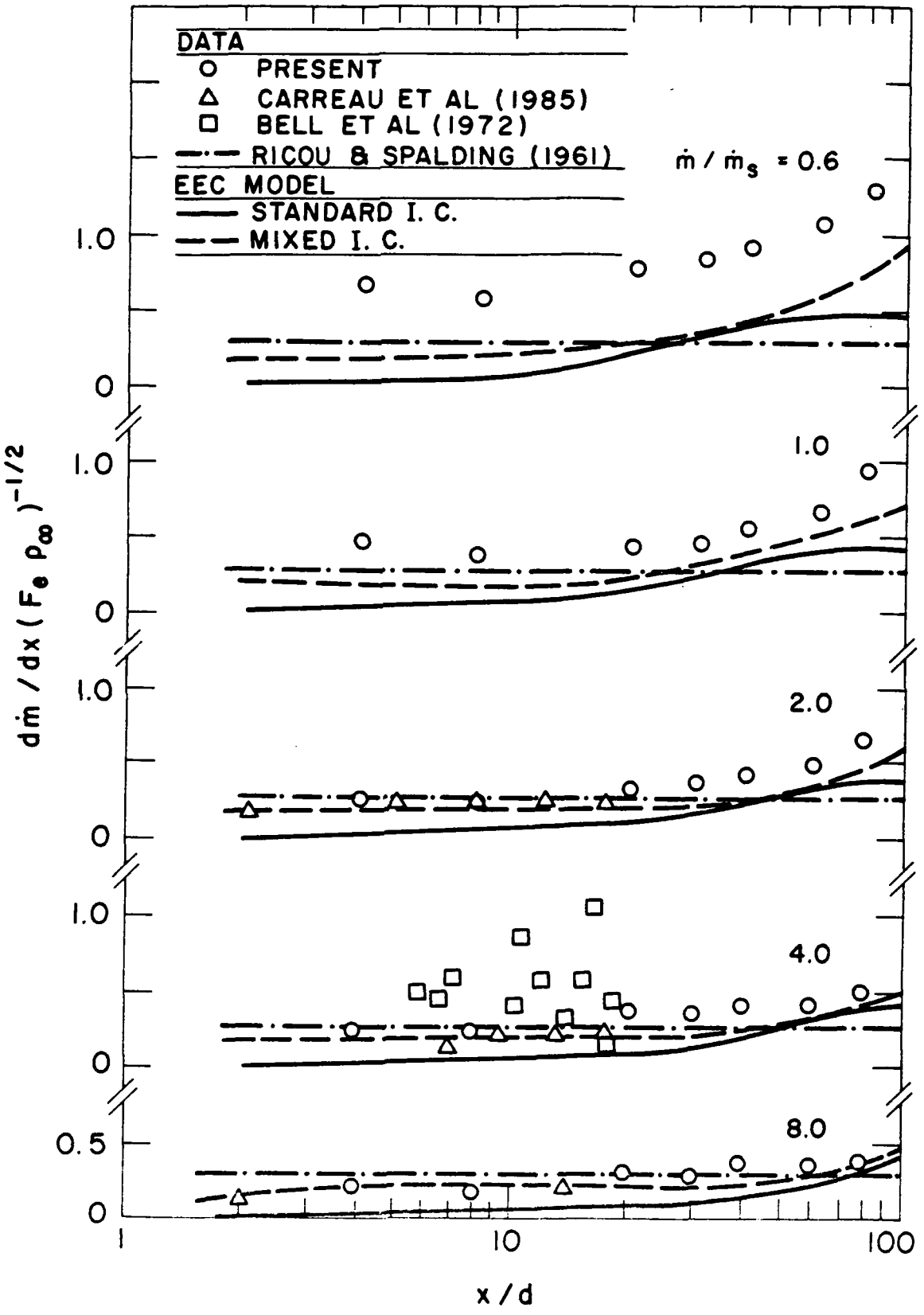

Figure 23. Streamwise variation of entrainment coefficient of round jets.

fully-developed portion of the flow, similar to the correlation of Ricou & Spalding (1961). Measured entrainment coefficients also increase everywhere as $\dot{m}/\dot{m}_s$ decreases. This probably due to enhanced mixing caused by increasing unsteadiness at low underexpansion ratios.

The comparison between predictions using standard initial conditions and the measurements, seen in Fig. 23, is generally poor, although predictions tend to improve as $\dot{m}/\dot{m}_s$ and x/d increase. Predictions using the mixed initial conditions, however, are in reasonably good agreement with the measurements except for $\dot{m}/\dot{m}_s = 0.6$ where predictions substantially underestimate the measurements. The behavior suggests that the discrepancies are largely due to enhanced mixing from effects of unsteadiness very near the jet exit. This is a major effect when the flow at the jet exit is subsonic but still persists to a significant degree for the underexpanded jets.

4.2.2 Plane Jets

Initial Conditions. Time averaged mean and fluctuating axial velocities were also measured for the plane jet in still air. The results are illustrated in Figs. 24 and 25. The plane converging nozzle was designed to yield a uniform exit velocity profile. The measured mean velocity profile is reasonably uniform except for the last ten percent near the jet edge. The variation of mean velocities near the jet edge is probably due to gradient broadening of the LDA measurements, since the size of the measuring volume is approximately equal to the distance between data points in this region. Note that since measurements were taken at an x/b position of zero, the expansion fan acceleration observed for the round jet (Loth & Faeth, 1987) is not observed. Results illustrated in Fig. 25 indicate a uniform turbulence level of about three percent but the spatial resolution is not adequate to detect the edge boundary layer. From these measurements, the nozzle appears to provide a uniform velocity profile with a relatively low turbulence intensity at the jet exit.

Void Fractions. Measurements of void fraction distributions were limited to the region $1 \leq x/b \leq 8$. Measurements were not undertaken at larger x/b since the rapid growth of the flow caused the flow aspect ratio to decline to two at $x/b = 8$ so that two-dimensionality is questionable farther downstream. Measurements and all predictions indicated a time-averaged void fraction along the axis of unity in the region where measurements were made; therefore, only void fraction distributions at various x/b will be considered in the following.

Measured and predicted distributions of time-averaged void fractions for $\dot{m}/\dot{m}_s = 1, 2, 3$ and 4 are illustrated in Figs. 26-29. Results are plotted as a function of y/x,

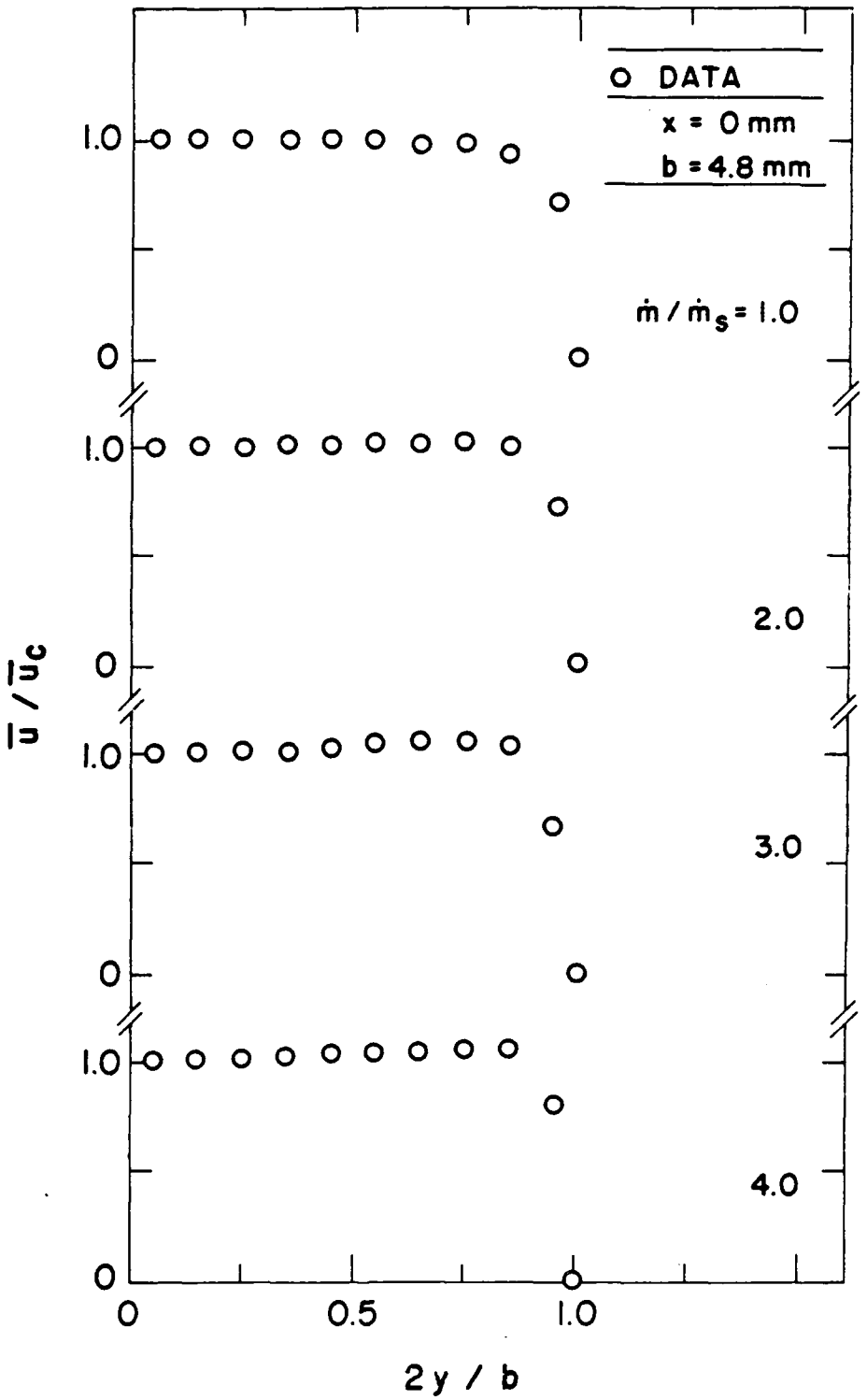

Figure 24. Streamwise mean velocities at exit of plane jets.

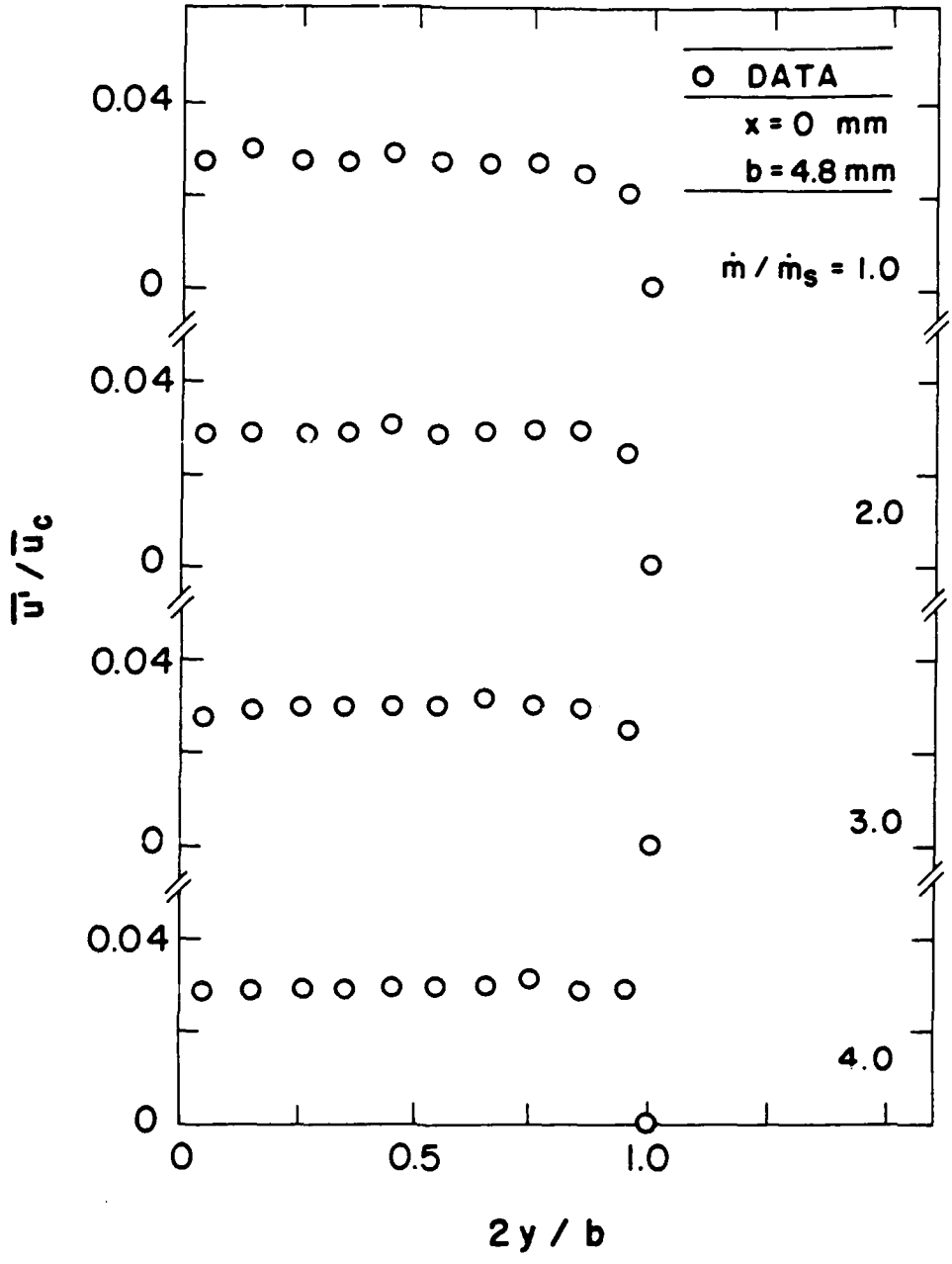

Figure 25. Streamwise velocity fluctuations at exit of plane jets.

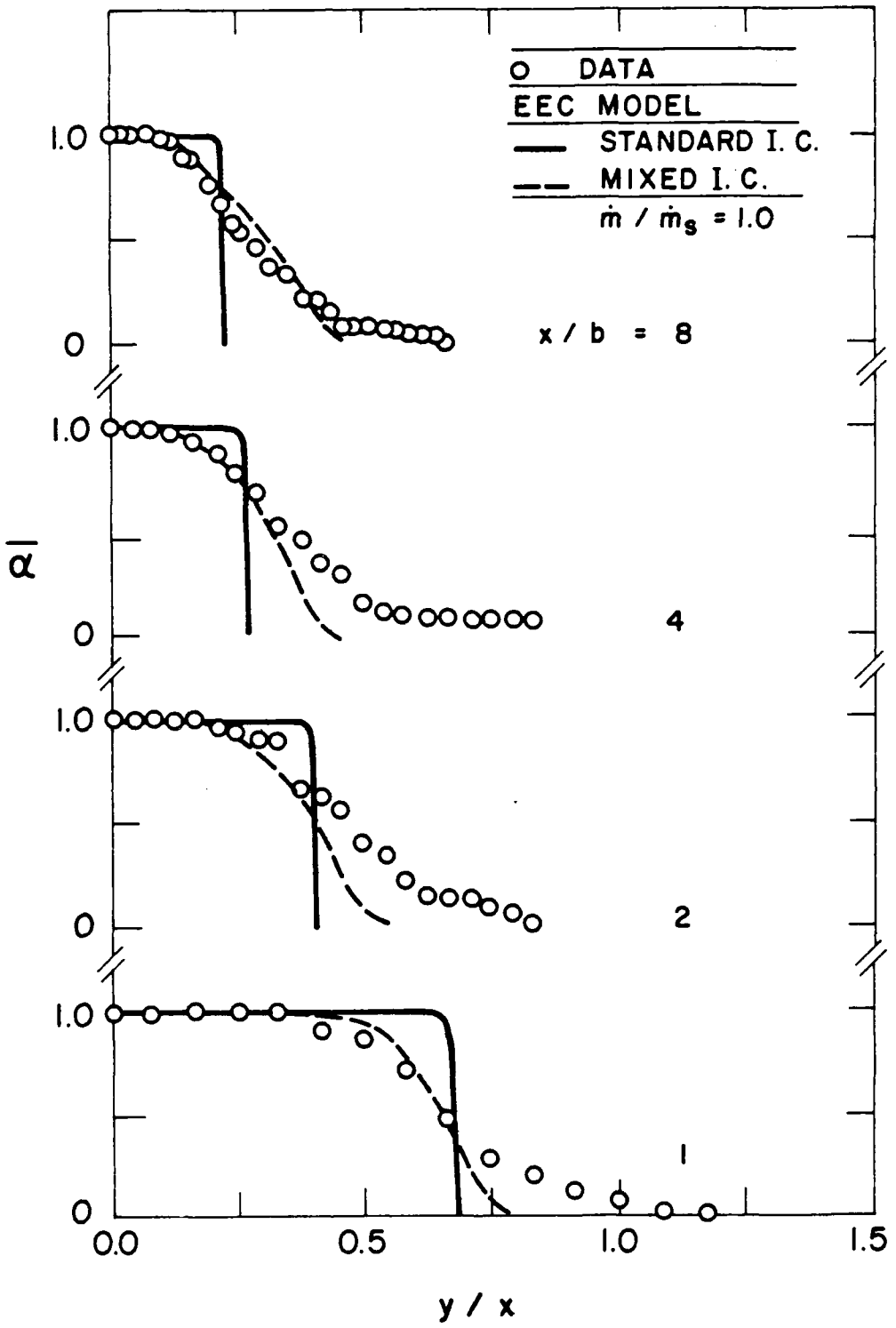

Figure 26. Time-averaged void fractions of plane jets for $\dot{m}/\dot{m}_s = 1.0$.

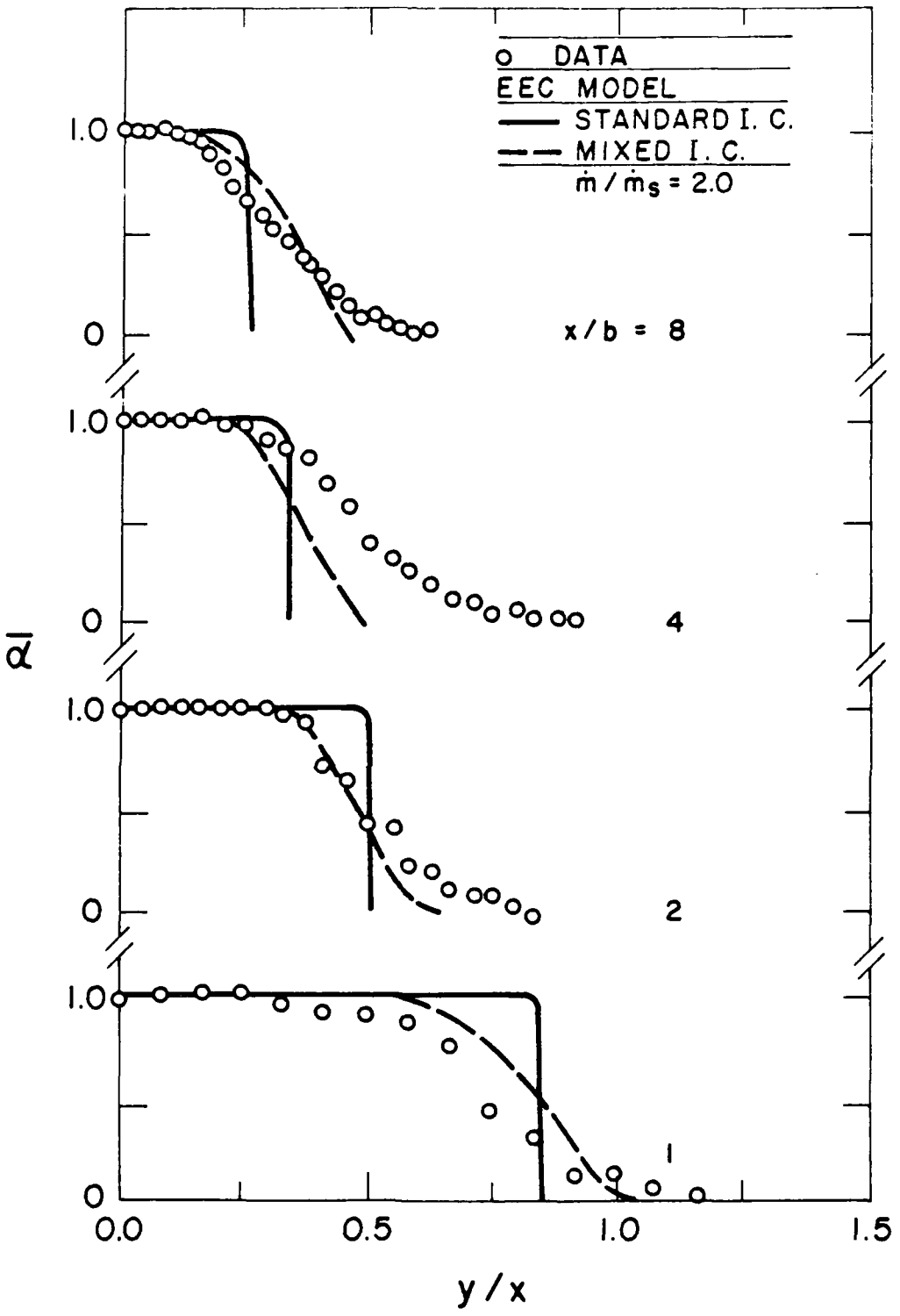

Figure 27. Time-averaged void fractions of plane jets for $\dot{m}/\dot{m}_s = 2.0$.

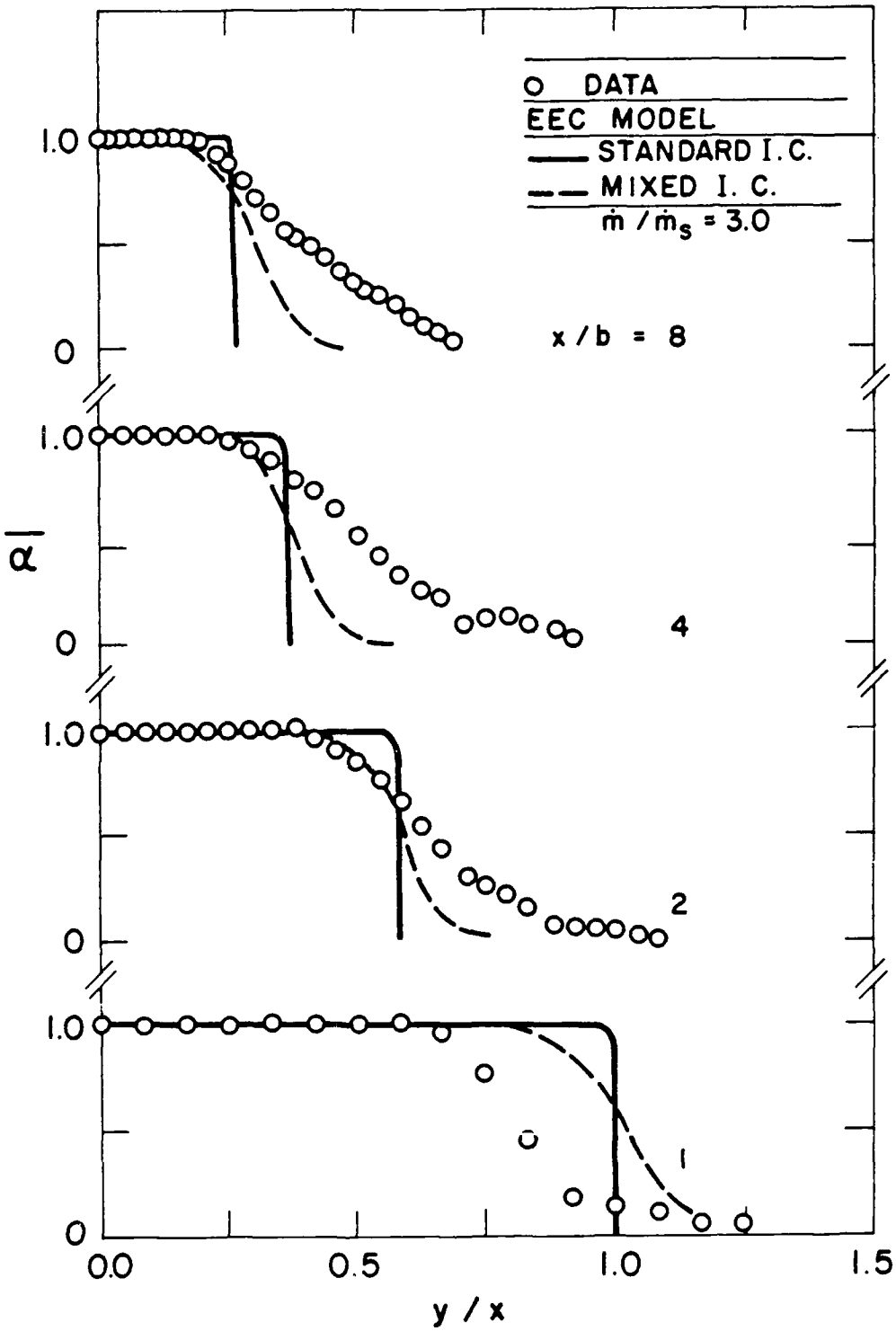

Figure 28. Time-averaged void fractions of plane jets for $\dot{m}/\dot{m}_s = 3.0$.

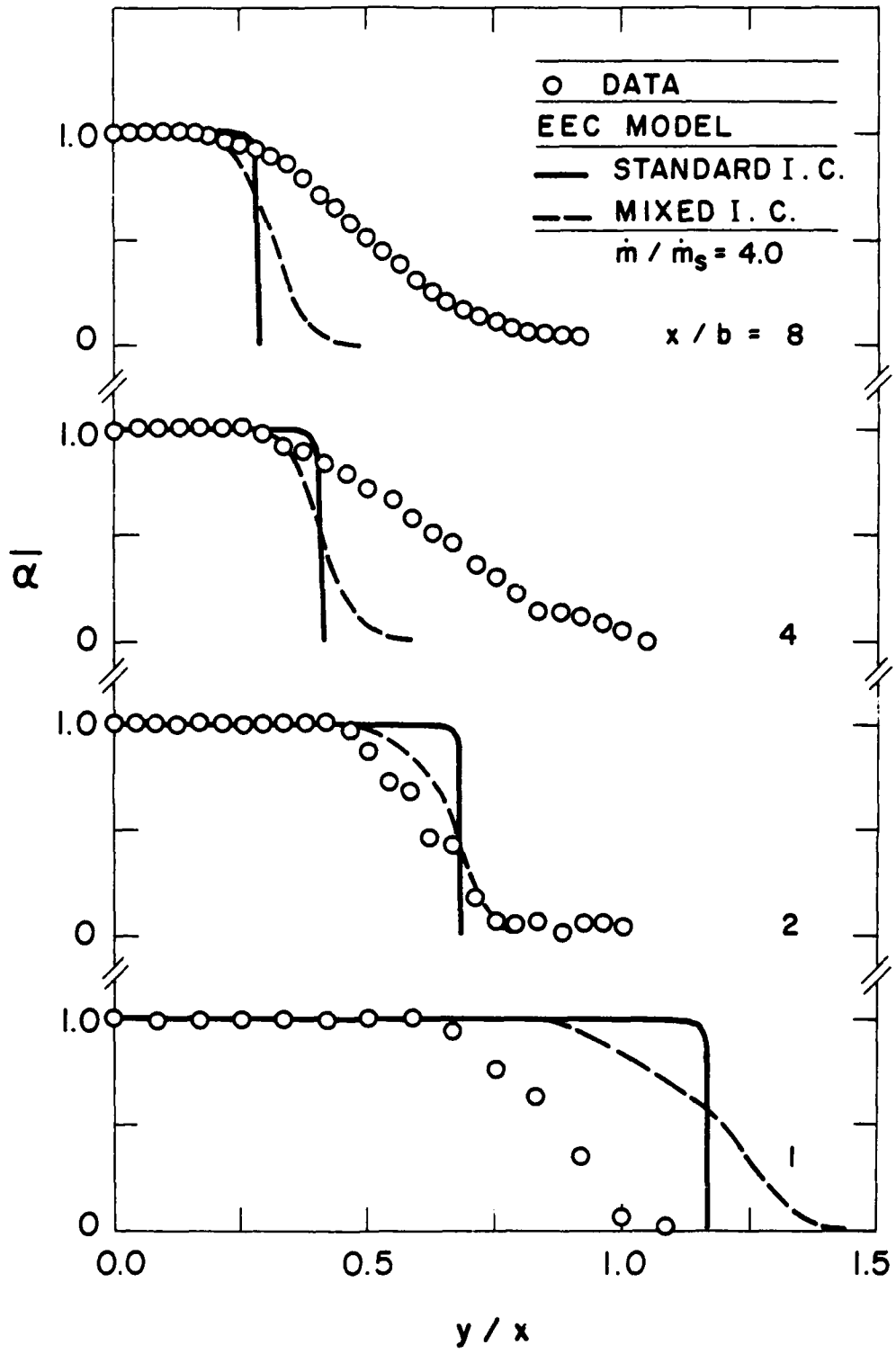

Figure 29. Time-averaged void fractions of plane jets for $\dot{m}/\dot{m}_s = 4.0$.

which is the similarity variable for the fully-developed region of plane turbulent jets and plumes. The predictions are based on the equivalent-adapted-jet approach (EEC model) using both standard and mixed initial conditions.

Similar to the round jet results, the most striking feature of the results illustrated in Figs. 26-29 is the large lateral widths of the void fraction profiles, ca. y/x of 0.5 as opposed to 0.15 for scalar property widths of single-phase flows. This behavior is partly caused by the fact that the near jet exit region is being considered where flow widths are invariably quite large when plotted in terms of y/x. However, the large sensitivity of void fractions to mixture fractions is also a factor, as pointed out in connection with the round jets. In general flow widths become narrower, in terms of y/x, with increasing x/b. This follows since the flow is still developing in the near injector region, e.g., the round jet results in Figs. 13-18 suggest that similarity would be approached at larger x/b.

The comparison between predictions and measurements for the sonic adapted jet, Fig. 26, is quite encouraging. Use of both the standard and mixed initial conditions yield a reasonably good estimate of the mean void fraction width of the flow and its development with increasing distance from the jet exit. Use of the mixed initial conditions, however, provides a superior estimate of the shape of the void fraction profile. This suggests enhanced mixing very near the injector exit, related to the near injector unsteadiness that was observed for both the round and plane jets. Once this is accounted for, however, subsequent mixing rates are not unusual in comparison to estimates based on the locally homogeneous flow approximation. This suggests that finite-rate interphase transport rates are not a major factor with respect to mixing rates in the near-injector region for adapted conditions.

Void fraction distributions for underexpanded conditions, shown in Figs. 27-29, involve additional complications due to the presence of the external expansion region. This introduces new sources of errors between predictions and measurements due to varying pressures in the flow field, seen in Fig. 9, which cause crosstream expansion and contraction of the mean position of the mixing layer. Naturally such features cannot be approximated by the adapted jet approximation even though this approach provides a crude representation of the mean position of the mixing layer.

Effects of the wave field of the external expansion region on crosstream mean void fraction distributions are evidenced by the apparently whimsical variations in the agreement between predictions and measurements (particularly when using the mixed initial conditions) as a function of distance from the jet exit and underexpansion ratio. For example, the agreement between predictions and measurements is generally quite

good for all underexpansion ratios at x/b = 2; predictions generally overestimate measured flow widths at x/b = 1; and predictions generally underestimate measured flow widths at x/b = 4 and 8. Furthermore, discrepancies at x/b = 1, 4 and 8 tend to increase as the underexpansion ratio increases. The reason for this behavior can be seen from the static pressure traces illustrated in Fig. 9. It happens that x/b = 1, 4 and 8 all fall near conditions where static pressure near the plane of symmetry is near the ambient pressure and is decreasing with increasing distance from the jet exit. This corresponds to positions where the outward deflection of the mixing layer surrounding the external expansion region is a maximum causing the flow to be wider than predictions ignoring the pressure field. Naturally this outward deflection increases as the underexpansion ratio increases, so that discrepancies between predictions and measurements increase with increasing underexpansion ratio. On the other hand, the position x/b = 2 corresponds to a minimum in the static pressure field along the axis, where the mixing layer is roughly halfway between its extreme positions - which fortuitously corresponds to the location predicted when the pressure field is ignored.

Lateral deflections of the mixing layers due to pressure variations can only be predicted by extending the analysis to consider the wave field, analogous to parabolized Navier-Stokes methods for underexpanded air jets in air (Chuech et al., 1988). However, use of the locally homogeneous flow approximation introduces very large density variations in the flow (ca. 1000:1) which makes it much more difficult to achieve stable and accurate solutions of the governing equations. Since parabolized Navier Stokes algorithms also require careful handling to assure stable and accurate results for even single-phase flows, extension of these methods to treat gas injection into liquids under the locally homogeneous flow approximation will not be a trivial matter - difficulties concerning the proper treatment of compressibility effects and shock wave interactions in a multiphase flow aside.

In addition to discrepancies just noted due to the external expansion region, differences of predictions between the standard and mixed initial conditions are roughly the same as for the round jets, with use of the mixed initial conditions providing superior predictions of the general shape of the void fraction mixing layer. This adds to evidence for unusual degrees of mixing near the jet exit, although the mechanism for this behavior has not yet been resolved.

Figure 30 is an illustration of predicted and measured characteristic flow widths (defined as twice the crosstream distance where $\bar{\alpha}/\bar{\alpha}_c = 0.5$) plotted as a function of x/b for various underexpansion ratios. These results illustrate the large width of the flow near the jet exit, which is expected due to flow development, with a trend toward an

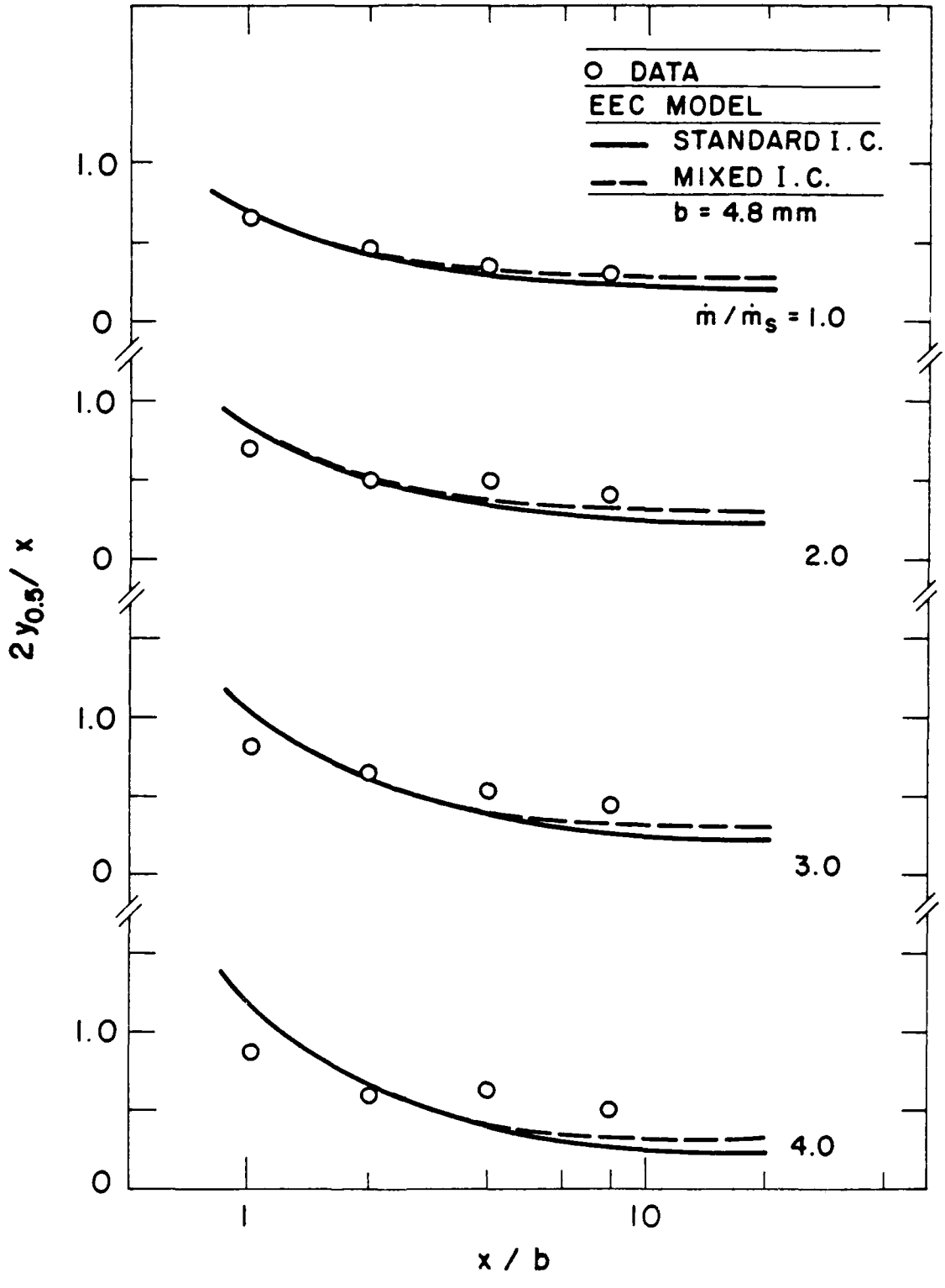

Figure 30. Streamwise variation of characteristic void-fraction flow width for plane jets.

asymptotic condition where the flow width is relatively independent of the distance from the jet exit at larger x/b. As noted earlier, however, this far field flow width is unusually large due to the influence of the large density ratio of the flow on the sensitivity of the void fractions to mixing levels. Similar to results for the round jets, the present approximate analysis yields reasonably good estimates of the characteristic flow widths and trends with respect to distance from the jet exit and the underexpansion ratio.

Entrainment. Predicted and measured dimensionless entrainment coefficients, based on equation (2.2), are plotted as a function of x/b for various underexpansion ratios in Fig. 31. An emperical relationship for gas injection into a still gas, due to Schneider (1985), is also plotted on the figure. Measurements exhibit a slight reduction in entrainment rates for increasing underexpansion ratios. This may be due to increased stability of the near injector region to flow unsteadiness, which was also noted in connection with the measurements for underexpanded round jets, see Fig. 23.

Another factor is that Mach numbers in the external expansion region increase as the underexpansion ratio increases: this would tend to reduce mixing rates analagous to well known effects of compressibility seen in supersonic shear layers (Papamoschou & Rosko, 1986; Bogdanov, 1983). The measurements also exhibit a progressive reduction in the dimensionless entrainment rate with increasing x/b, at all underexpansion ratios. This effect is largely due to transition of flow properties from nearly slug flow at the jet exit to fully-developed flow at downstream locations and can be found from the scaling laws for a fully-developed turbulent jet. Indeed, the empirical relationship due to Schneider (1985) for gas jets in still gases exhibits a similar trend, although quantitative agreement between this relationship and the measurements is not very good.

The comparison between predicted and measured dimensionless entrainment rates in Fig. 31, using the standard initial conditions, is generally not very good. This behavior can probably be attributed to unsteady features of the flow near the jet exit. This interpretation is supported by the fact that predictions using the mixed initial conditions provide very encouraging agreement with measurements, including trends with respect to both underexpansion ratio and distance from the jet exit. This result emphasizes the sensitivity of the flow to initial conditions and disturbances near the jet exit.

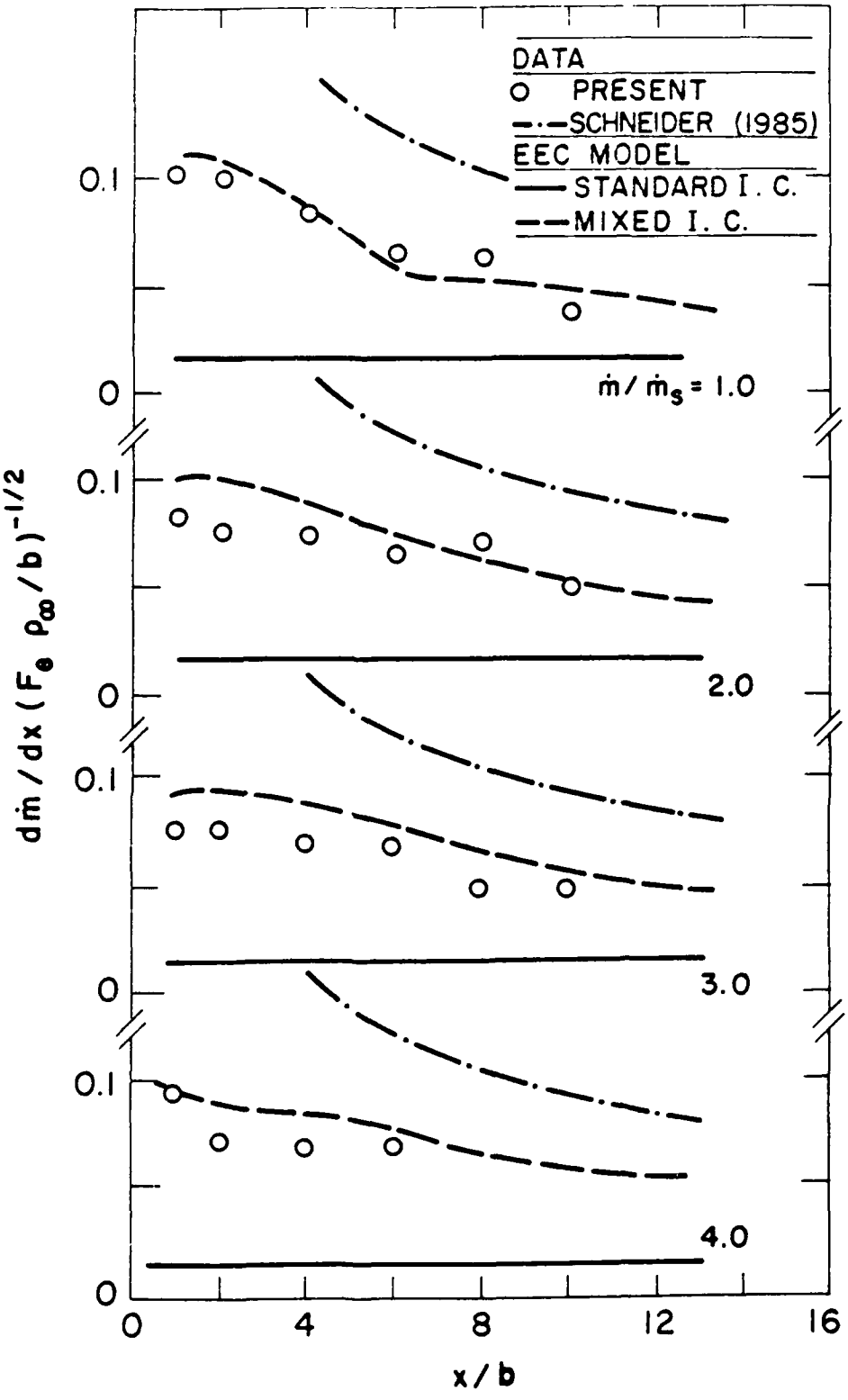

Figure 31. Streamwise variation of entrainment coefficient for plane jets.

5. Conclusions

Major conclusions of the present study are as follows:

1. Shock-wave-containing external expansion regions are present for underexpanded air jets in water but are smaller in extent than air jets in air for comparable conditions due to faster mixing rates. This behavior was established by both static pressure measurements and shadowgraphs which showed wave structure, complimenting earlier findings by Moiseev (1962) and Surin et al. (1983) based on dynamic pressure measurements.
2. Flow visualization showed that the mixing layer surrounding the external expansion region for plane air jets in water involved a bubbly region toward the liquid side and a drop-containing region toward the gas side, although significant stripping of drops only began near the downstream end of the first shock cell.
3. Effects of acoustic feedback observed for underexpanded air jets in air disappeared for underexpanded air jets in water at comparable conditions. This behavior is probably due to changed shock wave positions in the external-expansion region and different acoustic velocities and acoustic dampening in the multiphase mixing layer.
4. Air jets in water exhibit unusual flow widths based on void fractions due to the strong sensitivity of void fractions to mixing levels (mixture fraction), however, flow diameters based on dynamic pressures in round jets are more conventional.
5. Use of the locally-homogeneous-flow and effective-adapted-jet approximations yielded encouraging predictions of the properties of round air jets in water, particularly at large $\dot{m}/\dot{m}_s$ where effects of unsteadiness were reduced. The prescription of initial conditions for these calculations, however, had a significant influence on predictions of the shape of radial void fraction distributions and entrainment coefficients. Use of mixed initial conditions, to account for enhanced mixing due to unsteadiness near the jet exit, yielded best agreement with measurements.
6. Use of the locally-homogeneous-flow and effective-adapted-jet approximations were somewhat less successful for plane jets, where current measurements placed greater emphasis on the near-jet-exit region ($x/b \leq 8$). The main difference is that predicted lateral profiles of time-averaged void fractions were less satisfactory due to flow deflection by shock cells in the external expansion region which cannot be treated using the effective adapted jet approximation.

While the structure and mixing properties of the vertical underexpanded jets considered during the present study and by Tross (1974), and the horizontal underexpanded jets considered by Carreau et al. (1985), are predicted reasonably well using the mixed initial conditions, use of this prescription to allow for near-injector unsteadiness should be approached with caution. In particular, Surin et al. (1983) point out that condensing jets exhibit less unsteadiness than noncondensing jets while Loth (1988) found that even low levels of liquid coflow can significantly stabilize the flow as well. Clearly, a better understanding of the mechanism of unsteadiness near the jet exit, in the presence of a shock-wave-containing external-expansion region, is required to properly understand and reliably predict the properties of these flows.

References

Abdel-Aal, H.K., Stiles, G.B. & Holland, C.C. 1966 Formation of interfacial area at high rates of gas flow through submerged orifices. AIChE J. 12, 174-180.

Addy, A.L. 1981 Effects of axisymmetric sonic nozzle geometry on Mach disk characteristics. AIAA J. 19, 121-122.

Avery, J.F. & Faeth, G.M. 1975 Combustion of a submerged gaseous oxidizer jet in a liquid metal. Fifteenth Symposium (International) on Combustion The Combustion Institute, Pittsburgh, 419-428.

Bakaklevskii, Y.I. & Chekhovich, V.Y. 1978 Temperature field of a submerged stream jet. J. Engr. Phys. 34, 329-333.

Bell, R.B., Boyce, E. & Collier, J.G. 1972 The structure of a submerged impinging gas jet. J. British Nucl. Soc. 11, 183-193.

Bilger, R.W. 1976 Turbulent jet diffusion flames. Prog. Energy Combust. Sci. 1, 87-109.

Birch, A.D., Brown, D.R., Dodson, M.G. & Swaffield, F. 1984 The structure and concentration decay of high pressure jets of natural gas. Comb. Sci. Tech. 36, 249-261.

Birch, A.D., Hughes, D.J. & Swaffield, F. 1987 Velocity decay of high pressure jets. Comb. Sci. Tech. 52, 161-171.

Bilger, R.W. 1976 Turbulent jet diffusion flames. Prog. Energy Combust. Sci. 1, 87-109.

Bogdanoff, D.W. 1983 Compressibility effects in turbulent shear layers. AIAA J. 21, 926-927.

Borisov, A.A., Gelfand, B.E. & Timofeev, E.I. 1983 Shock waves in liquids containing gas bubbles. Int. J. Multiphase Flow 9, 531-543.

Carreau, J.L., Loukarfi, L., Gbakoue, L., Hobbes, P. & Roger, F. (1985) Hydrodynamics of an axisymmetric, submerged non-reactive gas jet-measurement of entrainment - contribution to the wastage modeling. Proceedings of the 19th IECEC American Nuclear Society, San Francisco, CA, Paper No. 859176, 1.688-1.695.

Chan, C.K. 1974 Dynamical pressure pulse in steam jet condensation. Proc. Fifth Intl. Heat Trans. Conf. ASME, New York, 3, 226-230.

Chen, L.-D. & Faeth, G.M. 1982 Condensation of submerged vapor jets in subcooled liquids. J. Heat Trans. 104, 774-780.

Chen, L.-D. & Faeth, G.M. 1983 Structure of turbulent reacting gas jets submerged in liquid metals. Combust. Sci. Tech. 31, 277-296.

Cho, D.H., Armstrong, D.R. & Bova, L. 1987 Dynamic behavior of reacting gas jets submerged in liquids: a photographic study. ONR Technical Report ANL 86-41.

Chuech, S.G. 1987 Kinematic and scalar structure of turbulent underexpanded sonic jets. Ph.D. Thesis, The Pennsylvania State University, University Park, PA.

Chuech, S.G., Lai, M.-C. & Faeth, G.M. 1987 Structure of sonic underexpanded turbulent air jets in still air. Interim Report, Navy Contract No. N00014-85-K-0604, Dept. Aerospace Engr., The University of Michigan, Ann Arbor, MI.

Chuech, S.G., Lai, M.-C. & Faeth, G.M. 1988 Structure of turbulent sonic underexpanded free jets. AIAA Paper No. 88-0700; also, AIAA J., in press.

Chun, J.H. & Sonin, A.A. 1984 Small-scale simulation of vapor discharges into subcooled liquid pools. National Heat Transfer Conference, Niagara Falls, NY.

Cumo, M., Farello, G.E. & Ferrari, G. 1978 Direct heat transfer in pressure-suppression systems. Proc. Sixth Intl. Heat Trans. Conf. ASME, New York, 5, 101-106.

Eggers, J.M. 1966 Velocity profiles and eddy viscosity distributions downstream of a Mach 2.2 nozzle exhausting to quiescent air. NASA TN D-3601.

Faeth, G.M. 1987 Mixing transport and combustion in sprays. Prog. Energy Combust. Sci. 13, 293-345.

Hinze, J.O. 1975 Turbulence. Second Edition, McGraw-Hill, New York, pp. 286-300, 715-742.

Jeng, S.-M. & Faeth, G.M. 1984 Species concentrations and turbulence properties buoyant methane diffusion flames. J. Heat Trans. 106, 721-727.

Kerney, P.J., Faeth, G.M. & Olson, D.R. 1972 Penetration characteristics of a submerged steam jet. AIChE J. 18, 548-553.

Kudo, A., Egusa, T. & Toda, S. 1974 Basic study on vapor suppression. Proc. Fifth Intl. Heat Trans. Conf. ASME, New York, Vol. 3, 221-225.

Lai, M.-C., Jeng, S.-M. & Faeth, G.M. 1986 Structure of turbulent adiabatic wall plumes. J. Heat Transfer 108, 827-834.

Lambier, G.R. & Chow, L.C. 1984 Pressure pulses during vertical and horizontal discharges of steam into subcooled water. National Heat Transfer Conference, Niagar Fall, NY.

Lee, L., Bankoff, S.G., Yuen, M.C. & Tankin, R.S. 1979 Local condensation rate in horizontal co-current steam-water flow. 18th National Heat Transfer Conference, San Diego, CA.

Limbaugh, C.C. & Kneile, K.R. 1984 Uncertainties propagation for combustion diagnostics using infrared band models. J. Quant. Spec. Rad. Trans. 31, 161-171.

Lockwood, F.C. & Naguib, A.S. 1975 The prediction of the fluctuations in the properties of free, round jet, turbulent diffusion flames Combust. Flame 24, 109-124.

Loth, E. 1988 Study of underexpanded turbulent air jets in water. Ph.D. Thesis, The University of Michigan, Ann Arbor, MI.

Loth, E. & Faeth, G.M. 1987 Noncondensing round turbulent gas jets in liquids. Department of Aerospace Engineering, The University of Michigan, Ann Arbor, MI.

Mahalingen, R., Limaye, R.S. & Brink, J.A., Jr. 1976 Velocity measurements in two-phase bubble-flow regime with laser-Doppler anemometry. AIChE J. 22, 1152-1155.

Moiseev, M.G. 1962 Discharge of a gas in a liquid through a Laval nozzle. Inzh. - Fiz. Zh. 5(91), 81-84.

Ohba, K., Kishimoto, I. & Ogasawara, M. 1977 Simultaneous measurements of local liquid velocity and void fraction in bubbly flows using a gas laser -- I. principals and measuring procedure. Tech. Rept. Osaka University 26, 547-556.

Ohba, K. 1979 Relationships between radiation transmissivity and void fraction in two-phase/dispersed flow. Tech. Rept. Osaka University 29, 245-254.

Papamoschou, D. & Roshko, A. 1986 Observations of supersonic free shear layers, AIAA Paper No. 86-0162.

Ricou, F.P. & Spalding, D.B. 1961 Measurements of entrainment by axisymmetrical turbulent jets. J. Fluid Mech. 11, 21-32.

Ruff, G.A., Sagar, A.D. & Faeth, G.M. 1988 Structure and mixing properties of pressure-atomized sprays. AIAA Paper No. 88-0237; also, AIAA J., in press.

Santoro, R.J., Semerjian, H.R., Emmerman, P.J. & Goulard, R. 1981 Optical tomography for flow field diagnostics. Int. J. Heat Mass Trans. 24, 1139-1150.

Schlichting, H. 1979 Boundary Layer Theory. McGraw-Hill, New York, p. 599.

Schneider, W. 1985 Decay of momentum flux in submerged jets. J. Fluid Mech. 154, 91-110.

Shapiro, A. 1954 Compressible Fluid Flow, Vol. 1, Ronald Press, New York.

Sherman, P.M., Glass, D.R. & Duleep, K.G. 1976 Jet flow field due to screech. Appl. Sci. Res. 32, 283-303.

Simpson, M.E. & Chan, C.K. 1982 Hydrodynamics of a subsonic vapor jet in a subcooled liquid. J. Heat Trans. 104, 271-278.

Soo, S.L. 1967 Fluid Dynamics of Multiphase Systems. Blaisdell Publishing Co., Waltham, MA.

Spalding, D.B. 1977 GENMIX: A General Computer Program for Two-Dimensional Parabolic Phenomena. Pergamon Press, Oxford.

Sun, T.-Y. & Faeth, G.M. 1986 Structure of turbulent bubbly jets - I. methods and centerline properties. Int. J. Multiphase Flow 12, 99-114; - II phase property profiles. Ibid., 115-126.

Surin, V.A., Erchenko, V.N. & Rubin, V.M. 1983 Propagation of a gas jet in a liquid. J. Engr. Phys. 45, 1091-1101.

Tross, S.R. 1974 Characteristics of a turbulent two-phase submerged free jet. M.S. Thesis, The Pennsylvania State University, University Park, PA.

Weimer, J.C., Faeth, G.M. & Olson, D.R. 1973 Penetration of vapor jets submerged in subcooled liquids. AIChE. J. 19, 552-558.

Wygnanski, I. & Fiedler, H. 1969 Some measurements in the self-preserving jet. J. Fluid Mech. 38, 577-612.

Young, R.J., Yang, K.T. & Novotny, J.L. 1974 Vapor-liquid interaction in a high velocity vapor jet condensing in a coaxial water flow. Proc. Fifth Intl. Heat Trans. Conf. 3, ASME, New York, 226-230.

ONR REPORT DISTRIBUTION LIST: CLOSED, LIQUID METAL COMBUSTION*

Dr. Gabriel D. Roy (2)
Mechanics Division, Code 1132 P
Office of Naval Research
800 N. Quincy Street
Arlington, VA 22217-5000

Dr. Richard S. Miller (2)
Mechanics Division, Code 1132P
Office of Naval Research
800 N. Quincy Street
Arlington, VA 22217-5000

Dr. Lynn A. Parnell
Naval Ocean System Center
Code 6341
San Diego, CA 92152-5000

Defense Documentation Center (12)
Building 5, Cameron Station
Alexandria, VA 22314

Technical Information Division (6)
Naval Research Laboratory
4555 Overlook Avenue SW
Washington, DC 20375

Dr. Jerry A. Smith
Chemistry Division
Office of Naval Research
800 N. Quincy Street
Arlington, VA 22217

Dr. Albert D. Wood
Technology Programs
Office of Naval Research
800 N. Quincy St.
Arlington, VA 22217

Dr. H.W. Carhart
Combustion & Fuels
Naval REsearch Laboratory
Washington, DC 20375

Professor Allen Fuhs
Department of Aeronautics
Naval Post Graduate School
Monterey, CA 93943

Division Director
Engineering and Weapons
US Naval Academy
Annapolis, MD 21402

Mr. Francis J. Romano
Code 63R3
Naval Sea Systems Command
Washington, DC 20363

Mr. Norman D. Hubele
Fluidic Systems, MS 1301-RR
Garrett Pneumatic Systems Division
2801 East Washington St.
Phoenix, AZ 85034

Dr. Hugh H. Darsie
Advanced Technology Group
Substrand Energy Systems
4747 Harrison Avenue
Rockford, IL 61101

Dr. Daniel H. Kiely
Power & Energy Group
The Pennsylvania State University
Applied Research Laboratory
P.O. Box 30
State College, PA 16801

Professor Darryl E. Metzger
Department of Mechanical and
Aerospace Engineering
Arizona State University
Tempe, AZ 85281

Dr. Dae H. Cho
Reactor Analysis & Safety Division
Argonne National Laboratory
Argonne, IL 60439

Professor S.H. Chan
Department of Mechanical Engineering
The University of Wisconsin-Milwaukee
P.O. Box 784
Milwaukee, WI 53201

---

* One copy except as noted in parenthesis.

Professor George A. Brown
Department of Mechanical Engineering
and Applied Mechanics
University of Rhode Island
Kingston, RI 02881

Professor A. Murty Kanury
Department of Mechanical Engineering
Oregon State University
Corvallis, OR 97331

Professor Irvin Glassman
Department of Mechanical and
Aerospace Engineering
Engineering Quadrangle
Princeton University
Princeton, NY 08544

Professor Norman Chigier
Department of Mechanical Engineering
Carnegie-Mellon University
Pittsburgh, PA 15213

Professor George Janz
Cogswell Laboratory, R306
Department of Chemistry
Rensselaer Polytechnic Institute
Troy, NY 12181

Dr. Leonard Leibowitz
Chemical Technology Division
Argonne National Laboratory
9700 South Case Avenue
Argonne, IL 60439

Professor John Tarbell
104 Fenske Laboratory
Pennsylvania State University
University Park, PA 16801

Professor Thomas E. Daubert
104 Fenske Laboratory
Pennsylvania State University
University State Park, PA 16801

Dr. J. Braunstein
Research Division
Oak Ridge Operations
Department E
Oak Ridge, TN 37831

Mr. Robert Tompkins
Code 36621, Bldg. 126T
Naval Underwater Systems Center
Newport, RI 02841

Mr. Maurice F. Murphy
Code R33, Room 4-1711
Naval Surface Weapons, White Oak
Silver Spring, MD 20910

Dr. Kurt Mueller
Code R10
Energetic Materials Division
Naval Surface Weapons Center,
White Oak
Silver Spring, MD 20910

Dr. Earl Quandt, Jr.
Code 2704
David Taylor Naval Ship
Research and Development Center
Annapolis, MD 21402

Mr. Richard Bloomquist
Code 2752
David Taylor Naval Ship R&D Center
Annapolis, MD 21402

Dr. Lawrence P. Cook
High Temperature Processes Group
National Bureau of Standards
Washington, DC 20234

Dr. W. Lee
Research and Technology Department
Naval Surface Weapons Center
Silver Springs, MD 20703

END
DATE
10-88
DTIC